Trabajo Fin de Grado en Física

Efecto Radiativo del Aerosol Atmosférico: Comparación entre Técnicas de Medida.

Radiative Effect of Atmospheric Aerosol:
Comparison between Measurement Techniques.

José Javier Fernández Carabantes

Universidad de Granada
Departamento de Física Aplicada

Julio 2023

Resumen

El aerosol atmosférico está constituido por partículas sólidas o líquidas en suspensión en la atmósfera terrestre, poseen un gran papel en el balance radiativo terrestre, pues pueden dispersar o absorber radiación. Este trabajo estudia la influencia existente al usar técnicas de teledetección o in-situ desde superficie, en las propiedades radiativas del aerosol atmosférico, en las estaciones atmosféricas de Granada y El Arenosillo (ambas en España). Se usan medidas de fotometría solar (teledetección pasiva) y de nefelometría integrante y fotometría de absorción (in-situ), obtenidas de bases de datos internacionales AERONET (AErosol RObotic NETwork) y WDCA (World Data Centre for Aerosols), respectivamente. Se caracterizan las diferencias en la interacción de los aerosoles con la radiación según el método de medición usado a partir del Albedo de Dispersión Simple (SSA), encontrando diferencias relevantes entre las capas atmosféricas superficiales (in-situ) y la columna atmosférica (teledetección) en caso de existir gran cantidad de aerosoles antropogénicos ligados a polución y actividad humana. En Granada, se encuentra predominancia de absorción en la superficie y de dispersión en el conjunto de la columna, mientras que en El Arenosillo la dispersión es dominante en toda la columna. Usando el Exponente de Ångström (AE) se estudia la predominancia del tamaño del aerosol, lo cual permite constatar el proceso predominante de interacción con la radiación y el origen de los aerosoles presentes según distintos métodos de medición. En Granada existe un gradiente significativo, dominando en superficie aerosoles finos, mientras que en El Arenosillo los aerosoles gruesos son predominantes en todas las capas. Se estudian las tendencias mediante el uso de tests estadísticos de Mann-Kendall y el estimador de Theil-Sen. Este análisis es realizado tanto para todos los datos existentes como los simultáneos, aplicando un filtro de simultaneidad en las bases de datos. Las tendencias de variables in-situ y de teledetección son coincidentes en su mayoría para la estación de Granada, ocurriendo lo contrario en El Arenosillo, siendo el principal motivo la falta de un rango temporal de estudio suficiente.

Abstract

Atmospheric aerosol is composed of solid or liquid particles suspended in the Earth's atmosphere, and it plays a significant role in the Earth's radiative balance as it can scatter or absorb radiation. This thesis examines the influence of using remote sensing or in-situ techniques at the surface, on the radiative properties of atmospheric aerosols, in the atmospheric stations of Granada and El Arenosillo (both in Spain). Measurements from solar photometry (passive remote sensing) and integrating nephelometry and absorption photometry (in-situ) are used, obtained from international databases AERONET (AErosol RObotic NETwork) and WDCA (World Data Centre for Aerosols), respectively. Differences in the interaction of aerosols with radiation are characterized based on the measurement method used, using the Single Scattering Albedo (SSA), significant differences are found between the surface atmospheric layers (in-situ) and the atmospheric column (remote sensing) in the presence of a large amount of anthropogenic aerosols associated with pollution and human activity. In Granada, there is a predominance of absorption on the surface and scattering across the column, whereas in El Arenosillo, scattering is dominant throughout the column. Using the Ångström Exponent (AE) the predominance of aerosol size is studied, which allows confirming the dominant process of interaction with radiation and the origin of the aerosols present according to different measurement methods. In Granada, a significant gradient exists, with fine aerosols dominating at the surface, while in El Arenosillo, coarse aerosols are predominant in all layers. Trends are studied using Mann-Kendall statistical tests and the Theil-Sen's estimator. This analysis is performed for both all existing data and simultaneous data, applying a simultaneity filter in the databases. The trends of in-situ and remote sensing variables mostly coincide for the Granada station, whereas the opposite occurs in El Arenosillo, primarily due to the lack of a sufficient temporal study range.

Agradecimientos

Este trabajo está realizado en inglés, pero quiero hacer mis agradecimientos en español pues no todas las personas que los merecen conocen ese idioma.

En primer lugar me gustaría agradecer a mi tutora D.ª Gloria Titos Vela y mi cotutor D. Alberto Cazorla Cabrera, por su disponibilidad, ayuda y guía a lo largo de estos meses en los que he realizado el trabajo aquí presente, agradezco su trato cercano y su confianza depositada al dejarme conocer un poco más cómo trabaja un físico en la vida real, conociendo el ambiente que existe en instalaciones de investigación como es la del IISTA-CEAMA, enseñándome a seguir el método científico, siendo crítico con los datos y resultados.

Agradecer también a todos mis compañeros de carrera que me han acompañado estos cuatro años, en especial a la F de Física, sin Juan Galván Paz y Pedro Jesús Lorente Molina lo más seguro es que hoy no estaría escribiendo estos agradecimientos, pues estaría estudiando otra carrera.

No puedo olvidarme de mis amigos y amigas del colegio mayor Cardenal Cisneros, que me han ayudado y soportado durante cuatro largos años quejándome de la carrera, pero que bien saben que preferiría que nunca se acabase. Destacar a mi fiel compañero de batallas Jaime Moreno San Antonio, futuro físico con el que he vivido tanto los mejores como peores momentos que la física puede darte, a Victor Vegas Luque, que ha sido mi veterano durante estos años y a Ángeles Fernández Jordán, que ha tenido que aguantar el desarrollo de este trabajo y siempre me ha apoyado. También agradezco a mi otra familia de amigos en mi tierra natal de Málaga, a los Mikes que pese a que partí allá por 2019 a estudiar fuera, siempre me han esperado con los brazos abiertos para un viernes de frías cuando podía regresar.

Por último y más importante, mi mayor agradecimiento va hacia mi familia, en especial a mis padres, por haberme permitido estudiar fuera sabiendo que la física era mi vocación e ilusión, por haber sido mi más firme pilar en estos años, por educarme y hacer de mí la persona que soy, por ello y mucho más les dedico este Trabajo de Fin de Grado.

Contents

1. Introduction

Nowadays, atmospheric aerosols have gained a higher degree of interest and concern in our society. Aerosols can be defined as both liquid and solid particles suspended in a gas, in our case the Earth's atmosphere [55]. Studying these particles presents challenges due to their high variability in time and location, with lifetimes ranging from days to weeks depending on their properties, formation processes, and geographical location [77].

Atmospheric aerosols have progressively gained greater importance as their implications in climate have been revealed. Aerosols alter the planet's energy balance, interact through scattering and absorption with incident radiation, and play a crucial role in atmospheric dynamics as cloud condensation nuclei, affecting precipitation. Numerous studies have been conducted to understand the principles of this balance, given its significant implications in the current situation of climate change and global warming [10], [11] & [32].

There is a significant amount of evidence that the radiative effect of aerosols results in a negative balance, meaning they cause a dominant cooling effect through scattering, reflecting the incident solar radiation back to space. This counters a substantial portion of the absorption caused by greenhouse gases (GHGs) [15]. Recent studies on this decreasing effect suggest that the current trend of reducing anthropogenic aerosol emissions in response to cleaner energy use in industry, transportation methods, and stricter regulations [64] & [9] will lead to aerosols having a predominantly absorptive radiative effect, thereby contributing to global warming [19] & [22].

However, there is still a significant uncertainty regarding the role of atmospheric aerosols in the radiative balance and their impact on climate, as evidenced in [20], [23] & [6]. This uncertainty stems from the considerable temporal and spatial variability of aerosols, which is reflected in current measurement techniques. In-situ measurement techniques provide high temporal resolution but lack spatial resolution as they primarily measure near the surface [12]. On the other hand, remote sensing techniques, including satellite-based observations using LIght Detection And Ranging (LIDAR) [28] and solar photometers, offer the advantage of studying the entire atmospheric column with high spatial resolution. However they have limited temporal resolution associated with the measurement technique, especially sun-photometers, resulting in biases in atmospheric climatology studies.

Despite the existence of numerous studies conducted in the past years using these measurement techniques (in-situ and remote sensing), at multiple sites around the world and covering large temporal scales [14], [15] & [16], most of them are performed with a particular technique due to the availability of certain instrument at the observatory or due to insufficient data within a common temporal range.

Although there are studies that compare measurements from both methods at specific locations such as [21] or [27], these studies are limited to a few specific measurement stations and insufficient time periods for an in-depth analysis. Moreover, these studies yield both similar and discordant results in the atmospheric variables of the studied aerosols when in-situ and remote sensing results are contrasted, highlighting the significant uncertainty that persists when comparing these techniques. This underscores the need to investigate the underlying differences between both methods when describing aerosol properties and their potential trends.

2. Theorical foundation

2.1. Atmospheric aerosol: sources, origin, size & effects

Atmospheric aerosols can be classified based on their relevant characteristics, physical properties, formation processes, origin, and their effects on both climate and human health [35].

2.1.1. Sources

Atmospheric aerosols can have both anthropogenic and natural origins in varying proportions, around 90% in terms of mass are of natural origin while in terms of numbers the vast majority of aerosols are human-related [78].

- Anthropogenic aerosols: These are aerosols originating from human activities, typically resulting from pollution such as vehicle exhaust (black carbon), burning of fossil fuels or related to industry, energy production, domestic heating or agriculture.
- Natural aerosols: These are caused by factors unrelated to human activities. Examples include products of volcanic activity [59], marine aerosols, dust particles, or biogenic particles (products of the activity of living organisms such as pollen). Of these types of naturally occurring aerosols, two of them are worth explaining in greater detail due to their importance:
  - Marine aerosols: These do not have an uniform concentration, they are more relevant in coastal areas but even present in inland locations despite not being products of continental plates [80]. They are generated by wind and ocean waves and are typically composed of sea salt, entering the atmosphere through sea spray.
  - Mineral dust aerosols: These are produced as a result of natural erosive effects and are predominant in arid and desert climates. Their characteristics vary greatly depending on the wind erosion mechanism [69]. Generally, most suspended dust is composed of elements such as silicon, calcium, aluminum, or magnesium, in compounds such as calcite [CaCO3] or dolomites [CaMg(SO3)]. In particular they are responsible of events of calima in the Iberian peninsula as well as other parts of the globe, calima is composed of carbonates, clays, quartz, iron and manganese oxides [68].

2.1.2. Origin

Properties of atmospheric aerosols can vary widely depending on their formation processes, aerosols can be divided in two main groups based on this fact [39] & [77]:

- Primary aerosols, are directly emmited into the atmosphere by physical or mechanical procedures. The main natural primary aerosols are sea salt and mineral dust as explained earlier. On the other hand black carbon (BC) is the main primary anthropogenic aerosol.
- Secondary aerosols, are produced via a gas-particle conversion process in the atmosphere. Volcanoes and biogenic aerosols due to sulfur emissions constitute natural secondary aerosols. Typical secondary anthropogenic aerosols include those formed from SO_2 emissions, biomass burning or derivatives from the energy production to enhance domestic heating systems.

2.1.3. Size

Another commonly used description of aerosols is in relation to their diameter D_p. The size of an aerosol is determined by its origin and formation process, and particles are usually classified as “fine” or “coarse” depending

on their size. Fine particles are typically those with $D_p < 2.5$ μm, while coarse particles are those with $D_p > 2.5$ μm [34]. The size of the particles depends on the formation process; if it occurs through gas-to-particle conversion, the particles will be fine, while if it occurs through mechanical processes such as wind erosion or sea spray, the particles will be coarse. Therefore in general terms, naturally produced particles are predominantly coarse, while human-related particles are predominantly fine [74].

It is important to note that atmospheric aerosol sizes follow a modal distribution Fig. 1.

These distributions are not always clear-cut, as they depend on instrumental resolutions. Current, more precise measurements allow for the study of particle distributions below 0.01 μm, revealing four modes of size distribution [66], [34] & [81]:

1. **Nucleation mode**: composed of particles with diameters smaller than 0.01 μm that undergo a process of nucleation.

2. **Aitken mode**: larger particles with diameters between 0.01 μm and 0.1 μm, consisting of both primary and secondary particles from the previous mode that have undergone coagulation.

3. **Accumulation mode**: diameters between 0.1 μm and 2.5 μm, produced by condensation of vapors in which the droplets grow in size (they can also originate from the coagulation of the previous modes [39]), they typically do not grow to larger sizes due to their growth rate decreasing as that of accumulation mode particles decreases. These particles are usually removed from the atmosphere through precipitation, as they serve as condensation nuclei for precipitations.

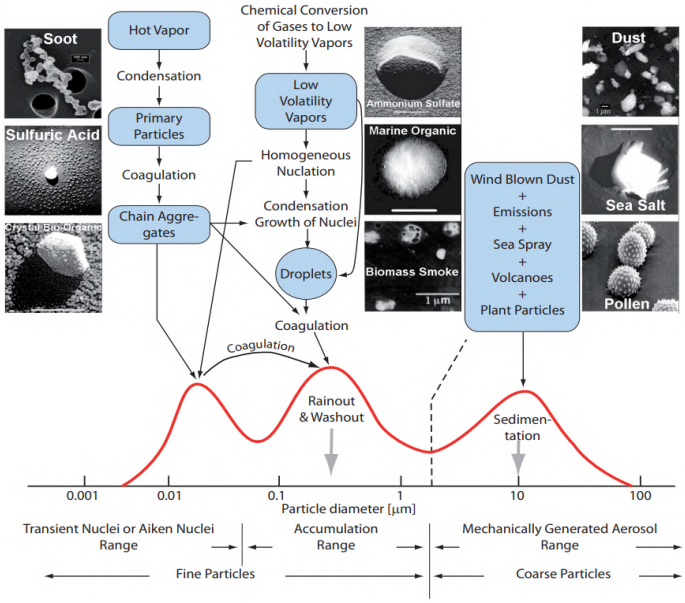

Fig. 1. Principal modes, sources, and particle formation and removal mechanisms shown for an idealized aerosol surface size distribution (taken from [63]). Shown are also examples images of single aerosol particles (taken from [54]).

4. **Coarse mode**: composed of particles larger than 2.5 μm, generally formed through mechanical disintegration processes. The typical mechanism of removal is by sedimentation.

2.1.4. Effects

Aerosols have a great impact in the atmosphere, their effects range from health concerns to climate change. Regarding the effects in human health, inhalation of anthropogenic aerosols such as black carbon or chemical products during variable term exposures can affect severely the health and well-being of the population, they can cause lung cancer, asthma, thrombosis or death in extreme concentrations or long enough exposure times [41], [18], [4],[5]& [39]. Not only anthropogenic aerosols can be dangerous to human health, but some natural aerosols such as polen can contribute to worsen the medical conditions in case of having an allergic response to them, crystalline silica or quartz (< 5 μm) are known to cause inflammation and fibrosis in the lungs and other organs [73].

The Intergovernmental Panel on Climate Change (IPCC) is the United Nations body for assessing the science related to climate change, it publishes reports regarding the causes and potentials impacts of climate change done by international collaboration [53].

In the IPCC report is stated the importance of aerosols in climate variation considering only the anthropogenic ones as causes of climate change [23]. These effects on the climate focus mainly on the variation of the Earth's energy balance. The radiative forcing is defined as a measure of the influence that a factor has in altering the balance of incoming and outgoing energy in the Earth's atmosphere system [20].

In Fig. 2 the change in effective radiative forcing since 1750 is shown.

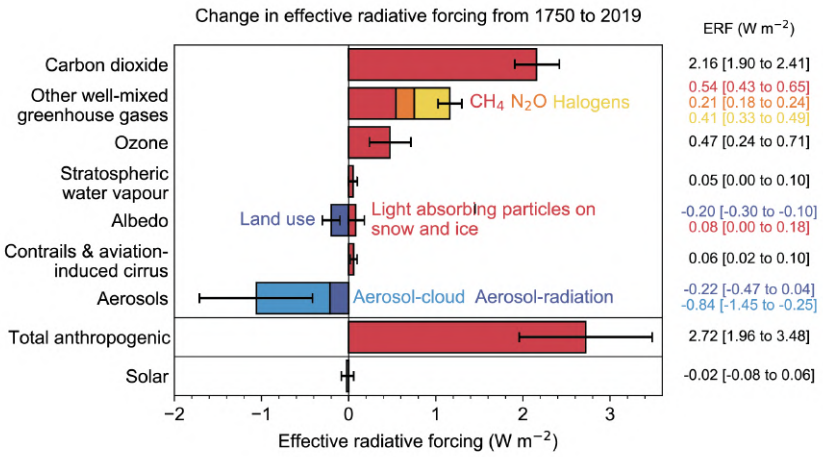

Fig. 2. Change in Effective Radiative Forcing (ERF) from 1750 to 2019 by contributing forcing agents (carbon dioxide, other well-mixed greenhouse gases (WMGHGs), ozone, stratospheric water vapour, surface albedo, contrails and aviation-induced cirrus, aerosols, anthropogenic total, and solar). A positive variation in effective radiative forcing indicates an increase in the net radiation absorbed by the Earth, which can lead to additional warming of the climate system, while a negative variation indicates a decrease. Taken from IPCC (2021) [6].

The radiative effect of anthropogenic aerosol in the atmosphere is about -0.5 Wm^{-2} with a likely range of -1.0 to -0.1 Wm^{-2}. This means that anthropogenic aerosols are exerting a cooling effect on the Earth's climate system. While the total aerosol radiative forcing, which includes both natural and anthropogenic aerosols is -1.1 Wm^{-2} in the range of -2.0 to -0.3 Wm^{-2}. However, the magnitude and sign of the radiative forcing can vary depending on factors such as the type of aerosol, its size and chemical composition, and its location and distribution in the atmosphere, which explains the presence of a high uncertainty in the ERF values [6].

2.2. Optical properties of the atmospheric aerosol: matter-radiation interaction

Consider a light beam that travels a distance through the atmosphere, the ray will be extinguished (partially or totally) by two processes that constitutes the interaction of light with particles suspended in the layer of atmosphere penetrated, those are the Absorption and Scattering processes.

2.2.1. Scattering and absorption coefficients (σ_{sp} & σ_{ap})

- Absorption constitutes a process in which the energy of the incident ray is transferred to the particle's internal energy. The absorption coefficient, $\sigma_{ap}(\lambda)$, informs about how absorbent is a particle.
- Scattering is a process where the incident ray is dispersed in all directions, the process can be elastic (the scattered ray has the same wavelength) or inelastic (the scattered ray's wavelength changes). The scattering coefficient $\sigma_{sp}(\lambda)$ describes how dispersant is a particle at scattering incoming light-rays.

Scattering and Absorption take place simultaneously in the process of interaction radiation-particle, therefore it is essential to define a magnitude that characterizes the relevance of each one relative to the total interaction, this is done via the Single Scattering Albedo (SSA) defined as [77]:

$$\mathrm{SSA}(\lambda) = \frac{\sigma_{sp}(\lambda)}{\sigma_{sp}(\lambda) + \sigma_{ap}(\lambda)} = \frac{\sigma_{sp}(\lambda)}{\sigma_{ep}(\lambda)}, \tag{1}$$

from its definition can be deduced that values of SSA ≈ 1 correspond with a dominance of the scattering process, while SSA ≤ 0.8 indicate a high influence of absorbing particles. Although both processes occur simultaneously, it is possible to determine predominances in the processes depending on the type of aerosol studied [49] & [79]:

- Scattering aerosols: sulfates, nitrates, ammonium and sea-salt particles.
- Absorbing aerosols: primarily BC, soil and mineral dust, and brown carbon (nitrated aromatics, polycyclic aromatic hydrocarbons...).

The sum of these processes constitutes the total extinction that undergoes a light beam through an atmosphere layer by interacting with particles. The treatment of this process can be understood with the Beer-Bouguer-Lambert law.

2.2.2. Beer-Bouguer-Lambert law

The Beer-Bouguer-Lambert law describes the amount of radiation intensity that is transmitted through a layer with a thickness x, the original beam has an intensity $I_{0\lambda}$ and the final one (after crossing the homogeneous material) I_λ, therefore:

$$dI_\lambda = -\sigma_{ep}(\lambda) I_\lambda dx\ , \tag{2}$$

$$I_\lambda = I_{0\lambda} e^{-\sigma_{ep}(\lambda)\cdot x}\ . \tag{3}$$

The extinction coefficient $\sigma_{ep}(\lambda)$ is given by Eq. 4, the resolution of the differential equation Eq. 2 leads to an exponential decrease in intensity with distance (x) traveled in the medium. This coefficient describes the total radiation-matter interaction that exists in the process.

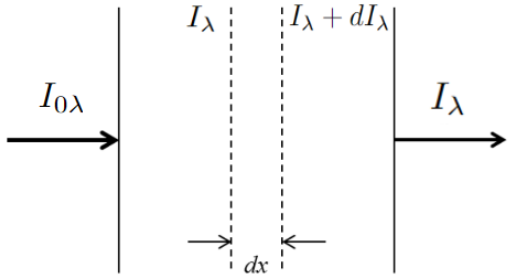

Fig. 3. Attenuation of radiation. Adapted from [77].

$$\sigma_{ep}(\lambda) = \sigma_{ap}(\lambda) + \sigma_{sp}(\lambda), \tag{4}$$

the extinction coefficient is therefore defined as the sum of all radiation-matter processes taking place, i.e., the sum of the scattering and absorption coefficients as expressed in Eq. 4, the unit of those coefficients is typically Mm^{-1}.

2.2.3. Aerosol Optical Depth (AOD)

The Aerosol Optical Depth (AOD) is an adimensional magnitude that reflects the attenuation capabilities of atmospheric aerosols of a determined wavelength λ light beam that traverses the atmosphere. It is possible to obtain its definition from the Beer-Bouguer-Lambert law (Eq. 3) [56]:

$$I_\lambda = I_{0\lambda} e^{-\tau_\lambda} \Rightarrow\ \tau_\lambda = \ln\left(\frac{I_{0\lambda}}{I_\lambda}\right) = \sigma_{ep}(\lambda)\cdot x \equiv \mathrm{AOD}\ . \tag{5}$$

Eq. 5 implies that the total AOD will be the sum of scattering and absorption contributions:

$$\tau_\lambda = \tau_\lambda(\text{scattering}) + \tau_\lambda(\text{absorption}) \,, \tag{6}$$

it can be interpreted as the total extinction accumulated over the whole atmospheric vertical column (referred to the zenit).

2.2.4. Spectral dependency: Ångström Exponent

As noted, the scattering and absorption coefficients as well as the AOD all have a dependency with the light's wavelength (λ), this spectral dependency is characterized by the Ångström Exponent, and can be defined for each one of the variables exposed before; providing valuable information about the aerosols' properties based on their values:

- The Scattering Ångström Exponent (SAE) gives the spectral dependency of the scattering coefficients, calculated from two wavelengths of interest λ_1 and λ_2 with Eq. 7:

$$\text{SAE}(\lambda_1 - \lambda_2) = -\frac{\log \sigma_{sp}(\lambda_1) - \log \sigma_{sp}(\lambda_2)}{\log(\lambda_1) - \log(\lambda_2)}. \tag{7}$$

  SAE can be used to identify the proportion of scattering done by fine and coarse particles, it increases with decreasing particle size and viceversa. It typically takes values ≈ 2 when it's dominated by fine and $\lessapprox 1$ by coarse particles [55] & [40].

- Absorption Ångström Exponent (AAE), analog to the SAE but referred to absorption Eq. 8:

$$\text{AAE}(\lambda_1 - \lambda_2) = -\frac{\log \sigma_{ap}(\lambda_1) - \log \sigma_{ap}(\lambda_2)}{\log(\lambda_1) - \log(\lambda_2)}. \tag{8}$$

  AAE gives an estimate of the different absorbent components present in the atmosphere and which is predominant, it takes values ≈ 1 for black carbon while ≈ 2 for mineral dust and/or organic aerosols [44].

- The AOD has an spectral dependence that can be expressed as well as Eq. 7 and Eq. 8 in terms of an Ångström exponent, able to be determined from two known wavelengths:

$$\text{AE}(\lambda_1 - \lambda_2) = -\frac{\log \tau(\lambda_1) - \log \tau(\lambda_2)}{\log(\lambda_1) - \log(\lambda_2)}. \tag{9}$$

  Just as SAE, the AE provides similar information about particles distribution sizes (due to scattering being typically the dominant process in the AOD), if AE $\lessapprox 1$ the measured aerosol is dominated by the coarse mode, otherwise if AE $\gtrapprox 2$ the size distribution is characterized by the fine mode [33].

3. Instrumentation

The instrumentation used for this study is based on three devices that measure and provide different type of data based on their characteristics and functional procedures. A distinction is made based on whether they measure using remote sensing techniques (column-integrated) or in-situ aerosols properties (surface).

The measurements in column are carried out using the entire atmospheric layer existing above the station level, for column measurements, solar photometers are used.
On the other hand in-situ instruments work only in their surrounding atmospheric layer, thus having a different study population resulting in differences in atmospheric variables' results of interest. Integrating nepehelometers and absorption photometers are used in this case, usually enclosed in a facility that provides samples of the surrounding atmospheric layer through a treated metal pipe to ensure the quality and minimize the losses in the air sample.

Apart from the use of different atmospheric layers in their respective measurements, there is an important bias when comparing both methods, in-situ measurements can be performed at any time of the day and regardless of the weather conditions. However, column measurements carried out by solar photometers, are only conducted when the Sun is visible in the sky. Additionally, it is only possible to take measurements when weather conditions allow (absence of clouds that hinder solar flux measurement in the column).

3.1. Solar photometer

As said, for remote sensing measurements a solar photometer (CIMEL CE318) is used, one can be seen in Fig. 4. It is designed as an automated way to obtain column measurements, where the measurement of Aerosol Optical Depth (AOD), is a direct measurement obtained by assessing the sun in a scheme dependent on the optical mass, which allows determining the solar flux loss between the upper layers of the studied column and the surface (expressed in Eq. 10) at various wavelengths such as 440, 670, 870, and 1020 nm. From these direct measurements, inversions are obtained, using different measurement schemes to obtain remote sensing variables such as SSA and AE (used in this study), as well as other variables such as refractive index or size distribution. These schemes measure the sky radiance and include the Almucantar sky (which measures radiance at azimuthal angles relative to the Sun) and the Principal Plane sky (which measures radiance at scattering angles in the solar principal plane away from the Sun). This type of measurement will result in a smaller amount of data compared to direct measurements [2].

Fig. 4. CIMEL CE318 [31].

$$\tau_\lambda = \frac{-1}{m_0} \ln \frac{F_\lambda}{\rho^{-2} F_{0\lambda}}, \tag{10}$$

in Eq. 10, m_0 is the optical mass, ρ is the relative distance between Earth and the Sun, F_λ and $F_{0\lambda}$ represents the solar fluxes, fist one being the ground level and second one on top of the atmosphere [42].

As said it is important to take into account that observations depend greatly on the climate and time of the day, this factor leads to a minor quantity of observations during the same time period compared to in-situ measurements.

3.2. Integrating Nepehelometer

Adapted from [77] & [76].

An integrating nepehelometer is an instrument able to obtain in-situ measurements of the light scattering coefficient σ_{sp} and the back scattering coefficient σ_{bsp}, throughout this work a model TSI 3563 (Fig. 5) is used providing results at three wavelengths 450, 550 and 700 nm.

This instrument blows an air sample to a volume inside itself, once inside, the sample is illuminated with a quartz-hallogen lamp over an angle of 7 to 170° (which constitutes a limitation in the total angles in light and back scattering, several correction techniques and calibration standards have been developed to address this issue, see [57].) The instrument measures the scattered lamp's light in those wavelengths by using three photomultiplier tubes (PMT) and dichroic filters (that split and direct the light scattered by the sample) set along the instrument's body, this light is directed into bandpass filters (red, green and blue) which provides the scattering coefficient at the desired wavelengths as seen in Fig. 6. This signal produced in the PMTs will be proportional to the intensity of the incident light, with the proportionality factor being the scattering coefficient.

To prevent scattering with the walls of the instrument, openings are used towards highly absorbent light traps combined with a highly absorbent coating on the internal walls of the device. This way it is possible to ensure that scattering occurs due to the air sample present in the study volume. Pressure and temperature are measured inside the volume where the light is scattered, to calculate the total scattering due to air molecules in order to be subtracted from the total scattering detected leaving the one corresponding to sorely the aerosols.

Fig. 5. Integrating Nephelometer (TSI 3563) [75].

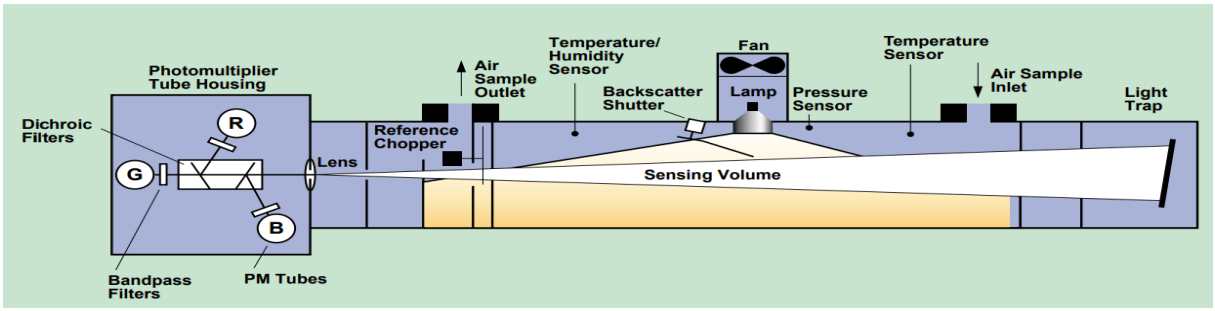

Fig. 6. Schematic representation of the TSI 3563 integrating nephelometer. Taken from [76].

3.3. Absorption photometer: MAAP & CLAP

An absorption photometer measures the absorption coefficient $\sigma_{ap}(\lambda)$ at different wavelengths depending on the model, throughout this work two different configurations with similar working fundamentals are used, MAAP THERMO 5012 and CLAP-10. A Multi-Angle Absorption Photometer is used (MAAP) Fig. 7, a 670 nm light source illuminates a filter with the aerosol sample. The absorption coefficients are determined from the radiative transfer considerations that include scattering effects and absorption enhancement due to reflections from the filter measured using photodetectors at two different angles (165 and 135°), the detected signal is converted into an electrical signal proportional to the light intensity to be processed in the data analysis phase [60] & [35]. A multi-angle standard calibration method is implemented [65]. A Continous Light Absorption Photometer (CLAP) has a similar frame of work. The CLAP measures light absorption of particles located in a filter, these particles are taken from the air layer of interest measuring the radiance transmission. The CLAP uses a solenoid valve that cycle through eight sample filter spots and two reference filter spots that are irradiated with a beam typically from a LED (the instrument is considered to work at ideal conditions having a filter transmittance greater than 0.7). Just as the MAAP, photodetectors are strategically placed to detect the transmitted fractions of the incident beam

of light [29]. The result data are the absorption coefficients at wavelengths 467, 528 and 652 nm and the standard calibration method implemented corresponds to the single angle correction [1].

a) Absorption Photometer (Thermo MAAP 5012) [72].

b) Absorption Photometer (CLAP-10) [52].

Fig. 7. Absorption photometers used.

3.4. Remote sensing data base: AERONET

The column data is obtained from AERONET (AErosol RObotic NETwork) [2], which is a is a federation of ground-based remote sensing aerosol networks established by NASA and PHOTONS, integrated by agencies, institutes, universities, individual scientists and partners. It has been operative for more than 25 years and imposes standardization of instruments, calibration, processing and distribution of data, being widely widespread across the globe as seen in Fig. 8.

In the AERONET database the data presents several levels of quality based on the filter and treatment they have received:

- Level 1.0: It is the most basic level, and the data uses the pre-field deployment sun calibration.
- Level 1.5: A cloud cleaning filter and an automatic quality check are applied to the level 1.0 data.
- Level 2.0: A final post-field calibration is applied to the level 1.5 data, representing the highest quality.

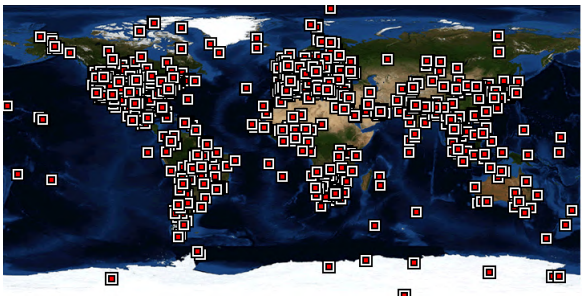

Fig. 8. Location of the stations integrated in AERONET.
Taken from [2].

This process results in real-time availability of data for levels 1.0 and 1.5, while level 2.0 data entails considerable delays resulting in a lower amount of available data. For this study, a quality level of 1.5 has been used.

3.5. In-situ data base: WDCA & ACTRIS

In-situ data has been obtained from the WDCA (World Data Centre for Aerosols) data base [3], which collects and manages aerosol-related data. Used as a repository of various organizations and scientists, playing a crucial role

in facilitating the exchange and sharing of different observations and meta data among researchers from all over the globe (Fig. 9), within the Global Atmosphere Watch (GAW) program of the World Meteorological Organization (WMO). This database not only provides aerosols raw measurements but also controlled and quality-assured data based on a rigorous standardization. In this database the ACTRIS (Aerosols, Clouds and Trace gases Research Infrastructure) base is employed, ACTRIS is a pan-european strategy of different European countries for aerosols' observations, clouds and gases making high quality observations [30].

A similar quality level distinction is present in this database as well, a level of 2.0 has been chosen for in-situ measurements, which are the scattering and absorption coefficients at various wavelengths depending on the instrument model.

Fig. 9. Location of the stations integrated in WDCA.
Adapted from [45].

4. Study sites

For this study two atmospheric observatories with instrumentation and available measurements in the databases of both measurements techniques have been used, shown in Fig. 10. These stations have significant differences in terms of climate, altitude, and human impact, which will be reflected when comparing the obtained results between them.

- Granada station (**UGR**) (37.164° N, 3.605° W, 680 m a.s.l).
  The Granada station is located within the city of Granada, in the facilities of the IISTA-CEAMA research institute. Granada is a medium-sized city with around 300,000 inhabitants (INE), located in the southern part of the Iberian Peninsula. It is not heavily industrialized but has one of the most air-polluted environments of Spain [46], and its climate features warm summers and cold winters. Additionally, the city is strongly influenced by its topography, surrounded by mountains of high elevation [38]. The instrumentation used in this station corresponds to a solar photometer (CIMEL CE318), an integrating nephelometer (TSI 3563) and an absorption photometer (MAAP 5012).

- El Arenosillo station (**ARN**) (37.104° N, 6.734° W, 41 m a.s.l).
  The El Arenosillo meteorological station is located in the southwest of the Iberian Peninsula in the province of Huelva. It is situated in a privileged location, far from major urban or industrial centers. The surrounding environment is rural and characterized by fine sandy beaches typical of its Atlantic location, as well as wetlands, with the notable presence of the Doñana National Park. The park influences the climate of the area, resulting in higher levels of humidity, localized precipitation, and variations in temperature and wind. The climate in the area is Mediterranean, with hot summers and mild winters [61]. The instrumentation used in this station corresponds to a solar photometer (CIMEL CE318), an integrating nephelometer (TSI 3563) and an absorption photometer (CLAP-10).

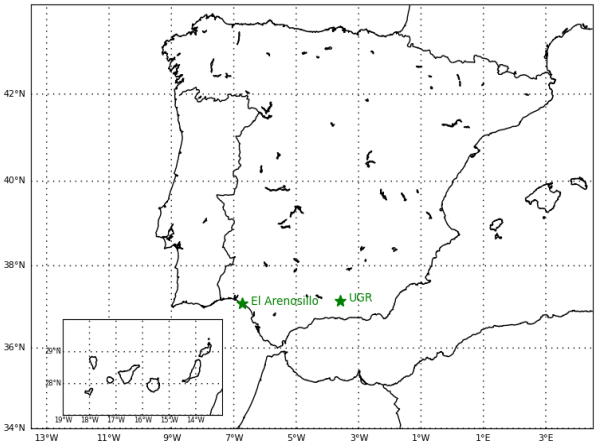

a) Location of the stations in Spain.

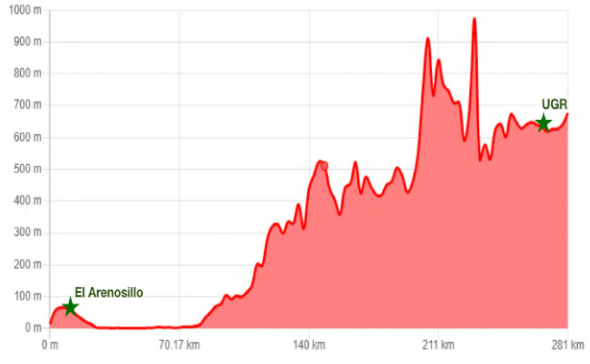

b) Topographic profile, altitude is presented in the y-axis while the longitudinal distance appears on the x-axis.

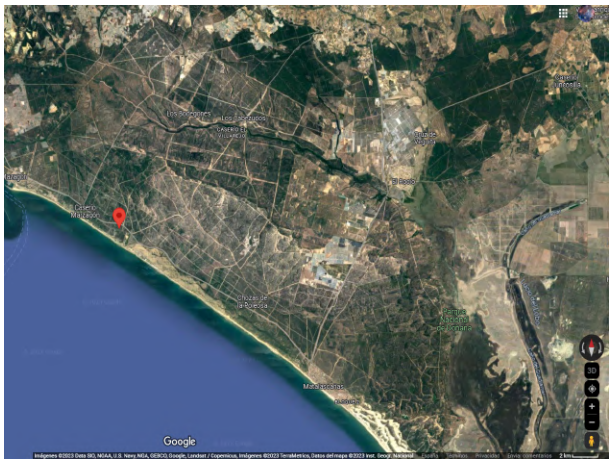

c) Satellite image of El Arenosillo (Google).

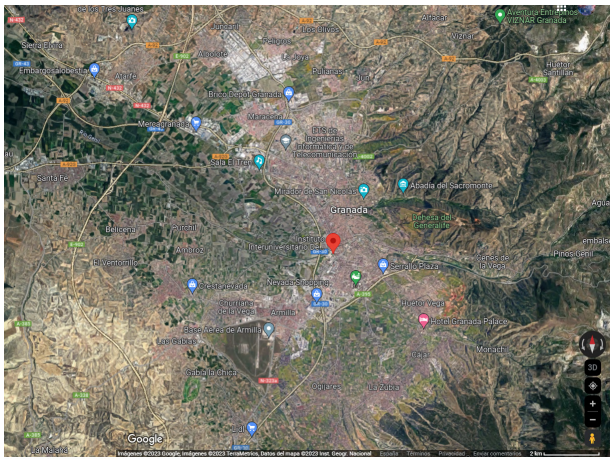

d) Satellite image of Granada (Google).

Fig. 10. Maps and topography of the stations used in the study.

5. Methodology

This section outlines the methodology followed while conducting this study, specifying the treatment of available data and the criterion used in obtaining the presented conclusions.
The Python programming language was used in Jupyter Notebooks along with the Pandas library, designed for the analysis of scientific data. The programs used can be found on appendix (8) where a further disquisition is exposed.

5.1. Analysis of databases: remote sensing & in-situ data comparison

Firstly, data from both remote sensing (AERONET) and in-situ (WDCA) databases were obtained, aiming to maximize the range of years with available measurements for both types with a minimum requirement of 5 consecutive years as shown in Table 1.

Station	AERONET	WDCA (Int. Nephelometer)	WDCA (Ab. Photometer)	Studied period
Granada	2004-2023	2006-2021	2006-2021	2006-2021
El Arenosillo	2001-2023	2008-2022	2012-2022	2012-2022

Table 1. Measurement period available for each measurement method (in years), and range of years chosen for the joint study at each station.

Initially, all available data from the databases have been obtained, i.e., the widest range of years available for each measuring instrument. The final study period has been defined as the intersection of these ranges, i.e., the maximum range of overlapping years in which measurements are available for all instruments.

Large time intervals have been identified where no measurements are present, either because the measuring instruments were out of service for calibration or due to measurement failures. In El Arenosillo station, this fact is even more pronounced for the measurements of CIMEL CE318 and its inversions, despite the large range of years appearing in the AERONET database. The instrument was not present at the station from 2010 to 2015, causing a lack of data for those years.

In addition to this first comparison between in-situ and remote sensing using the whole database, an additional filtering was applied to ensure measurements were taken at the same temporal instance for both measurement techniques. This was done to investigate the influence of measurement bias in sun-photometer measurements compared to in-situ measurements, as mentioned above, sun-photometer measurements are not continuous as they are restricted to day-time and cloud-free conditions, while in-situ measurements are performed continuously.

Henceforth, the term **simultaneous data** will refer to those data that have undergone the simultaneity bias of measurement methods, while **total data** will refer to those that do not have this filtering.

Measurement Method	AOD	SSA	AE	SAE	σ_{sp}	σ_{ab}	σ_{ep}
Column	✓	✓	✓				
In-situ		✓		✓	✓	✓	✓

Table 2. Aerosols' variables that have been studied, the tick indicates which measurement technique provides it.

Station	AOD	SSA_{Col}	SSA_{Situ}	AE	SAE	AAE	σ_{sp}	σ_{ap}	σ_{ep}
Granada	1020, 870 675, 440	1020, 870 675, 440	670	440-675	450-700	-	450, 550 700	670	670
El Arenosillo	1020, 870 675, 440	1020, 870 675, 440	670	440-675	450-700	528-652	450, 550 700	467, 528 652	670

Table 3. Wavelengths in **nm** of the studied variables, for AE (Ånsgtröm Exponent), AAE (Absorption Ångström Exponent) and SAE (Scattering Ångström Exponent), the two wavelengths used to calculate them are indicated according to their respective expressions.

In Table 2 the variables associated with each studied measurement method are indicated. Therefore the variables that can be compared between measurement techniques are the SSAs and AE/SAE.

5.2. Interpolation of wavelengths

To obtain the scattering and absorption coefficients at 670 nm wavelength (see Table 3[1]), it is necessary to interpolate using the variables SAE (scattering) or AAE (absorption).

In order to interpolate the scattering coefficient the SAE is calculated using Eq. 7 with wavelengths of 450 nm and 700 nm. The coefficient is calculated at these wavelengths and treated as constant within the wavelength interval. It is possible to express the spectral relationship of the scattering coefficient through the SAE in an alternative way using a parameter β called turbidity coefficient [8]:

$$\sigma_{sp}(\lambda) = \beta\lambda^{-\mathrm{SAE}} \Rightarrow \log(\sigma_{sp}(\lambda)) = \log(\beta\lambda^{-\mathrm{SAE}}) = -\mathrm{SAE} \cdot \log(\lambda) + \log(\beta). \tag{11}$$

Manipulating Eq. 7, we can solve for the scattering coefficient at the desired wavelength:

$$\sigma_{sp}(\lambda_2) = \frac{\sigma_{sp}(\lambda_1)}{(\lambda_1/\lambda_2)^{-\mathrm{SAE}}} \qquad \text{Where } \lambda_1 = 450 \text{ nm } \& \ \lambda_2 = 670 \text{ nm}. \tag{12}$$

Therefore, we can interpret it as a slope and consider it constant if the wavelength to be interpolated is close to the ones used to calculate it.

For the absorption coefficient the AAE (calculated from the wavelengths at 528 and 652 nm) is used. Taking into account that it is also possible to define:

$$\sigma_{ap} = \beta\lambda^{-\mathrm{AAE}}, \tag{13}$$

in a completely analogous way, it will be considered, with similar justification as in the previous case, that the value of AAE remains constant if the wavelengths used in the calculation are close to the one being interpolated. By rearranging Eq. 8, we can obtain the absorption coefficient:

$$\sigma_{ap}(\lambda_2) = \frac{\sigma_{ap}(\lambda_1)}{(\lambda_1/\lambda_2)^{-\mathrm{AAE}}} \qquad \text{Where } \lambda_1 = 652 \text{ nm } \& \ \lambda_2 = 670 \text{ nm}. \tag{14}$$

For the Granada station, only the scattering coefficient needs to be interpolated, this is done via Eq. 12, except for the year 2017, as a calibration issue was found within the integrating nephelometer for the red wavelength (700 nm), resulting in erroneous scattering coefficient measurements.

Since this affects the calculation of the SAE, SSA and the scattering coefficient at 670 nm, it was decided to calculate the interpolation using the wavelengths at 450 and 550 nm in Eq. 7 solely for this year, which entails an additional approximation in the process.

Whereas at El Arenosillo station, interpolation is needed for both scattering and absorption coefficients, using Eq. 12 and Eq. 14.

[1] $\mathrm{SSA_{Situ}}$ is referred to in-situ while $\mathrm{SSA_{Col}}$ to remote sensing (column) measurements.

5.3. Trend analysis

The methodology used in this study is based on a simplification of the one found in [14]. This trend analysis will be conducted for both total and simultaneous data in order to compare the results obtained.

To perform the analysis, a series of statistical tests implemented in the Python library "pyMannKendall" will be used [50]. The Mann-Kendall (MK) tests are used for the statistical analysis of data series that exhibit clear upward or downward trends. They provide the level of statistical significance of potential underlying trends. It is a non-parametric test, making it suitable for any type of non-normalized data. To determine the existence of these trends, the p-value with 95% confidence is used as the statistical goodness-of-fit coefficient in all cases. Specifically, if a p-value of less than 0.05 is obtained, it will be considered statistically significant (**ss**).

An important detail to consider is that the data series should not exhibit serial correlations (relationship between successive values of a time series). Due to the nature of most atmospheric processes, there is often positive correlation in the studied data. Therefore, numerous authors have developed pre-whitening tests to address this issue and avoid the introduction of statistical biases. Pre-whitening tests involve modifying the original MK test. In addition to determining statistical significance, a technique is applied beforehand (depending on the method used) to remove autocorrelation from the data. This pre-whitening process allows for a more accurate and reliable assessment of the potential existing trends [13].

It is also necessary to define the concepts of type 1 error and type 2 error since the tests have been implemented to minimize them and assess the evolution of the different results of (**ss**) found.

- Type 1 error: constitutes an increase in the probability of rejecting the null hypothesis of no statistical trend, that is, it is associated with false positives.
- Type 2 error: constitutes an increase in the probability of accepting the null hypothesis of a statistical trend, that is, it is associated with false negatives.

Within this context, three Mann-Kendall tests implemented are:

1. Original MK test [58]: This is the most basic of the tests as it does not perform pre-whitening. It is a solid test but presents an inflation of type 1 error in the case of autocorrelation.
2. Trend-free pre-whitening procedure (TFPW) [83]: This test does perform prewhitening of the data prior to the MK test. It does not present type 1 error but loses the ability to adjust to the trend due to a high type 2 error.
3. Variance-corrected trend-free pre-whitening procedure (VCTFPW) [82]: This test is the most powerful of the three implemented, allowing for an improvement in trend estimation and significantly reducing type 1 and type 2 errors.

The three tests have been implemented for each variable in the study. To determine the existence of a trend over a time period, the following criterion is used:

The VCTFPW test has been taken as the indicator of statistical trend due to its greater capability. The TFPW and original MK tests are also used to verify the presence of the aforementioned errors and how data correlation influences their results. According to the framework of [14], an annual (**ss**) existence is considered if, when studying by seasons (winter, spring, summer and autumn), the slopes and trends are homogeneous among themselves. If one season does not exhibit it while the others do, the existence of a statistical trend is considered if the annual trend is homogeneous with the seasons in which it is present.

Once statistical trends have been identified, it is necessary to characterize them using a regression method that provides a slope for the variable's trend. This is where several methods have been tested with varying results. Initially, the choice was to use least squares regression (LMS), but the results did not align with the actual trends.

The reason for this discrepancy is the presence of outliers, which are data points that do not correspond to the statistical trend and hinder the regression calculation. Therefore, the decision was made to implement the Theil-Sen's estimator, which is a method specifically designed for studying atmospheric trends where outliers are common due to rapid changes in the atmosphere (i.e. changes in emissions, atmospheric conditions, air masses...) or experimental setup errors.

The Theil-Sen's estimator method [48] & [67], differs from other regression methods in that it is based on the differences between pairs of data points rather than individual values. The procedure uses these differences between (x, y) values and sorts them based on the x value. The medians of these sorted differences represents the estimated slope of the regression line. This approach to calculating the regression slope is robust and prevents extreme values from incorrectly altering the trend of the population used [37].

In the study of data, representations of box plots (Fig. 11) will be used. This format is employed due to its ability to handle and display the available data population and its distribution for each variable. It is frequently used, particularly in the field of atmospheric physics. Based on a representation of the data values in quartiles [36]:

- The width of the box corresponds to the interquartile range, i.e., from the value Q1 (25%) to the value Q3 (75%) of the data, allowing to study the statistical dispersion of the data population.
- The whiskers extend from the box to the maximum and minimum values, conventionally located at 1.5 times the interquartile range.
- The median is represented by the solid line and represents the value Q2 (50%) of the data. If it is not located in the middle of the box, it indicates an asymmetry in the data distribution. The graphs will also display the number of observations located at this point and the value of the data mean (dashed line).
- Outliers are data points that fall outside the range defined by the whiskers' maximum and minimum values. They are considered atypical and frequently excluded from the analysis.

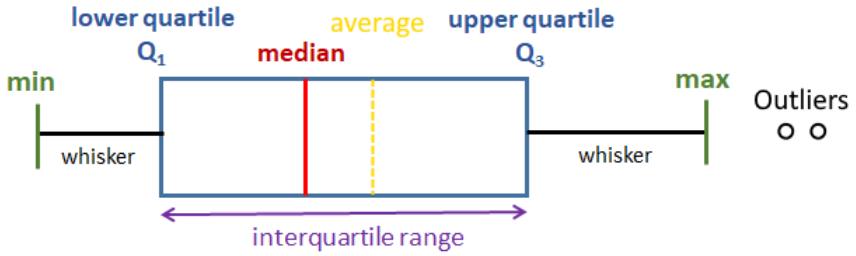

Fig. 11. Example of a box plot with its main aspects stated. Adapted from [62].

6. Results and discussion

6.1. Radiative balance: comparison between methods and measurement stations

According to the methodology explained, the variables of SSA (Single Scattering Albedo) and AE/SAE (Ångström Exponent and Scattering Ångström Exponent), will be compared for both measurement techniques, aiming to obtain information on how the measurement technique affects the information that can be extracted from the aerosol's properties according to theoretical fundamentals presented before.

First, in Fig. 12 & Fig. 13, both SSAs are compared for each station.

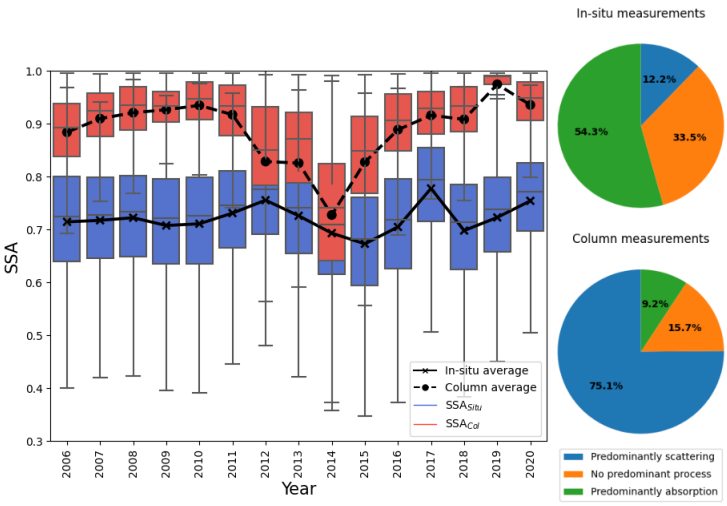

Fig. 12. SSA values and percentages of scattering and absorption taking place in Granada.

The box plots along with the mean values are presented, and the average values are the following: at Granada station $\mathrm{SSA_{Col}} = 0.9 \pm 0.1$ and $\mathrm{SSA_{Situ}} = 0.7 \pm 0.1$ both in close agreement to the ones found in [25] and [43] respectively, whereas at El Arenosillo station, SSA yields much more similar values between methods, $\mathrm{SSA_{Col}} = 0.94 \pm 0.07$ and $\mathrm{SSA_{Situ}} = 0.91 \pm 0.06$ close to the ones found in [47].

In both cases, higher SSA values are observed for column measurements compared to in-situ techniques. This indicates a predominance of scattering processes over absorption, as the SSAs are close to unity. Therefore, for remote sensing techniques, the aerosols can be identified predominantly as those that produce greater scattering than absorption, primarily marine aerosols or biogenic aerosols (such as pollen, found in lower layers of the column). The values obtained from the in-situ technique are lower than those from the column technique, indicating a lower proportion of scattering in the near-surface atmospheric layer compared to the upper layers, with values that indicate a predominance of absorption, evidencing that absorbing aerosols are mostly emitted near the surface.

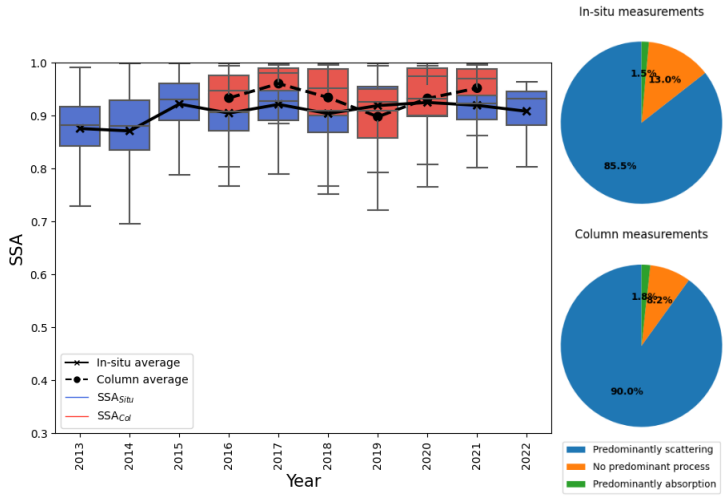

Fig. 13. SSA values and percentages of scattering and absorption taking place in El Arenosillo.

Comparing both measurement sites, in El Arenosillo, although the in-situ technique yields lower values, in-situ and remote sensing results are closer than in Granada, where the differences are far more profound, evidencing in this station that a higher proportion of absorbing aerosols in the near-surface layer is present compared to El Arenosillo. As seen in the pie charts, there are greater differences in the radiation-matter interaction processes between the surface layers and upper atmospheric layers in urban environments than in rural environments. This is attributed to the presence of black carbon (BC) and other anthropogenic aerosols, which are characteristic of vehicle emissions and other human activities more prevalent in the urban environment of Granada than in the vicinity of the Doñana natural park.

For AE (column) and SAE (in-situ), the results we can obtain by comparing both methods are related to the predominant size of aerosols, higher values of SAE/AE indicate a majority of fine type aerosols, on the contrary lower values represent a coarse mode majority, a relationship with the observed SSA can also be established (as in general, fine aerosols can be identified with a predominance of absorption while coarse with a majority of scattering processes [71]). In Fig. 14 & Fig. 15, the comparisons are shown. Obtaining for the station in Granada: SAE = 1.6 ± 0.5 and AE = 1.2 ± 0.5, that fall within the uncertainty range of those found by authors previously in [43] and [26], following a similar relationship. For the station in El Arenosillo: SAE = 1.3 ± 0.5 and AE = 1.1 ± 0.4 in close agreement to the ones presented in [24].

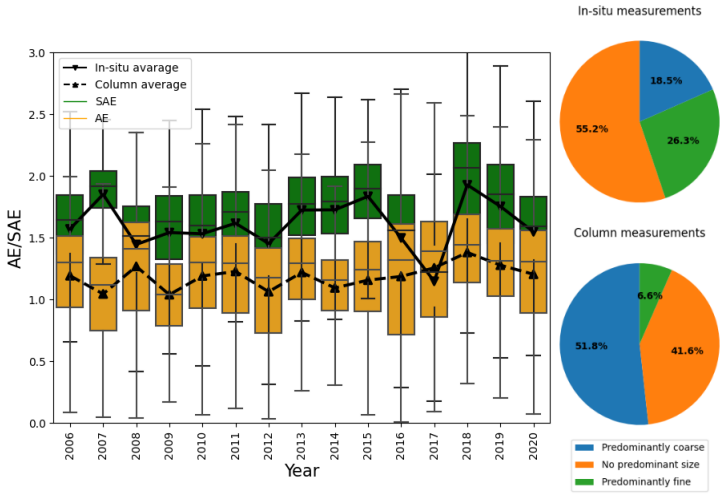

Fig. 14. SAE and AE values compared with the percentages of aerosol's size mode in Granada.

In both stations higher values are observed for SAE (measured near the surface) than AE (whole atmospheric column), which again indicates a notable differences in the dynamics of aerosols and their predominant type in the different atmospheric layers as well as between the studied stations.

Therefore in the upper layers there is a higher presence of larger-sized aerosols (coarse mode) such as marine spray or mineral dusts (in a lesser proportion, this last one is associated with sporadic phenomena), which present a larger predominance of scattering than absorption (as observed in the higher SSA in columnar measurements than in in-situ measurements), the proportions are presented in the pie charts, showing indeed the mentioned majority of coarse mode aerosols (majority of scattering processes) for column measurements.

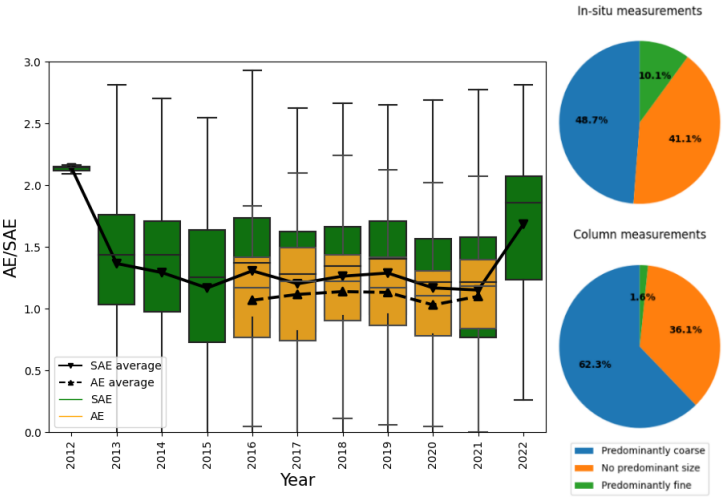

Fig. 15. SAE and AE values compared with the percentages of aerosol's size mode in El Arenosillo.

In the surface layers, the higher values of SAE compared to AE in both cases indicate a greater presence of more absorbing fine aerosols compared to the upper layers. This suggests the presence of anthropogenic fine aerosols, mainly black carbon (BC) among others such as sulphates or nitrates, by-products of human activities. When comparing the two stations, this phenomenon is more pronounced in Granada, where there is a higher proportion of fine aerosols in the surface layer. In contrast, in El Arenosillo, although the proportion of fine aerosols is higher than in the upper layers, it does not surpass the proportion of coarse aerosols pointing out a predominant scattering dominance in all layers, shown by the fact that the SAE values are closer to the AE values in El Arenosillo, compared to the station in Granada Fig. 15. Hence, once again, it is evident that the differences between measurement techniques and atmospheric layers are accentuated in urban environments[2].

[2]To determine predominant sizes or radiation-matter prevalences, the limits for SSA and SAE/AE exposed in 2.2.4 are used.

Lastly, although the AOD measurements correspond to column data and the extinction coefficient measurements are in-situ and do not directly correspond to a direct comparison, we can use the comparison of both to study if there are significant changes in the behavior between the surface layer and the upper atmospheric layers in Fig. 16, as the extinction coefficient σ_{ep}^{670} determines the AOD value as explained in Eq. 5.

For the Granada station, AOD has been found to have an average value of AOD $= 0.11 \pm 0.09$ in agreement to the ones found in [7], with a behaviour that generally corresponds to the one found in the coefficient. However, although the values are generally followed, locally this is not the case. For example, in the years 2007 or 2015, there are localized increases in σ_{ep}^{670} while this does not occur in AOD, thus evidencing the difference in proportion and composition of aerosols in the upper layer.

In the El Arenosillo station, the lack of available columnar data is evident due to technical problems as explained before, AOD presents values of AOD $= 0.09 \pm 0.12$ in accordance with those found by other authors in [24], but with a higher uncertainty than the AOD value itself due to the aforementioned lack of available data. In Fig. 16 a similar correlation between the surface layer extinction coefficient data and the upper layer AOD data is found.

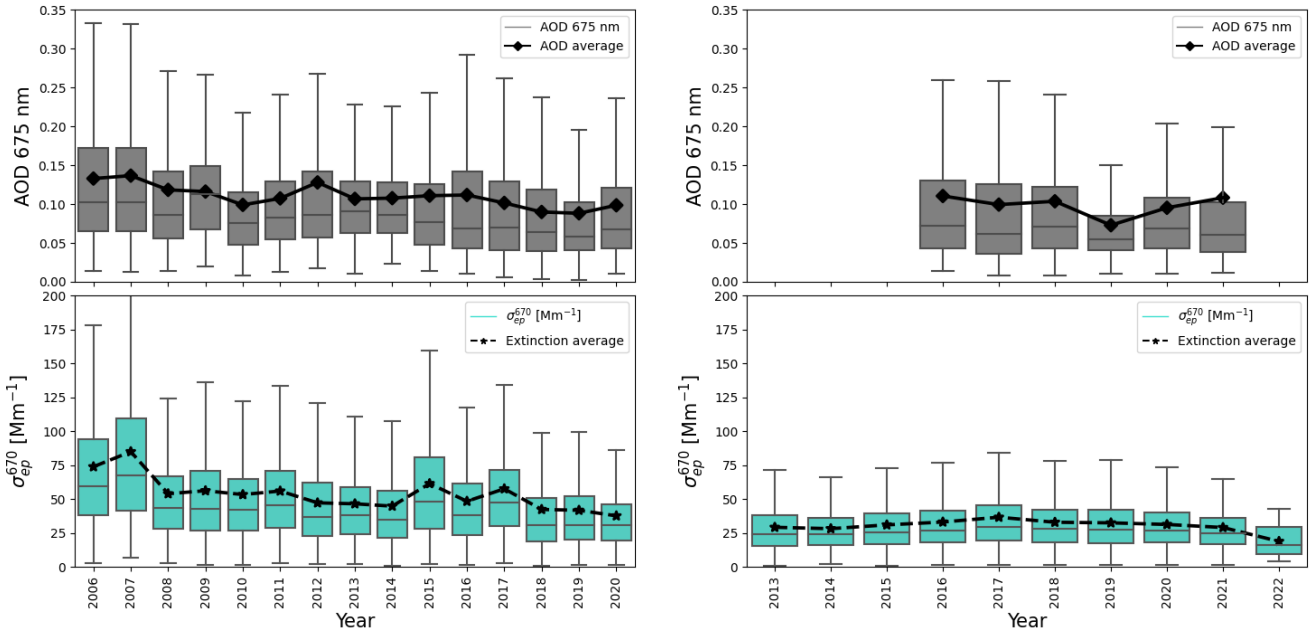

a) Granada. **b)** El Arenosillo.

Fig. 16. AOD and extinction values compared for each station.

6.2. Trend analysis: total and simultaneous data.

6.2.1. Total data

Using all available data in the studied time periods, matrices of data with daily measurement per month (y-axis) and day (x-axis) for each year in both stations are presented in Fig. 17 (Granada) and Fig. 18 (El Arenosillo). As expected, there are more in-situ measurements than column measurements, which increase in the central months of each year due to improved weather conditions (absence of clouds) and more hours of visible sun.
Four plots are shown per station, one for the integrating nephelometer and another for the absorption photometer, as although both in-situ instruments are capable of continuous measurement, they do not always provide the same number of measurements due to maintenance processes or measurement errors. Also two matrices are used to study the column data, one for the CIMEL's direct measurements (AOD) while the other one represents the explained inversions (SSA and AE), note how despite being done by the same instruments the inversions present far less measurements and have to be taken into account when applying the simultaneity filter as they will hinder considerably in-situ's number of available data once applied the simultaneity filter.

In fact when this simultaneity filter is applied, a single data frequency plot will be obtained for all instruments and variables in the study Fig. 23.

In figures Fig. 19, Fig. 20, Fig. 21 & Fig. 22 following the observed data matrices, the trends of the variables are studied for both stations. For this purpose, the explained methodology is followed, applying the Man-Kendall statistical tests and utilizing the Theil-Sen's estimator to obtain slope values[3]. The graphs also display the number of observations for each year located at the median values, in order to properly assess the identified trend.
The trends results are presented in Table 4, where I indicates a monotonic increasing trend, D a decreasing one and NT in case of a non-existing trend while the tests used are nicknamed in short: MK1 = Original Mann-Kendall test, MK2 = TFPW, and MK3 = VCTFPW. The final statistical significance of the variable is presented in a box under the column SS.

[3] All of the obtained slopes have units of $[\text{yrs}^{-1}]$ except the ones corresponding to the scattering, absorption and extinction coefficients which are expressed in $[\text{yrs}^{-1}\cdot\text{Mm}^{-1}]$.

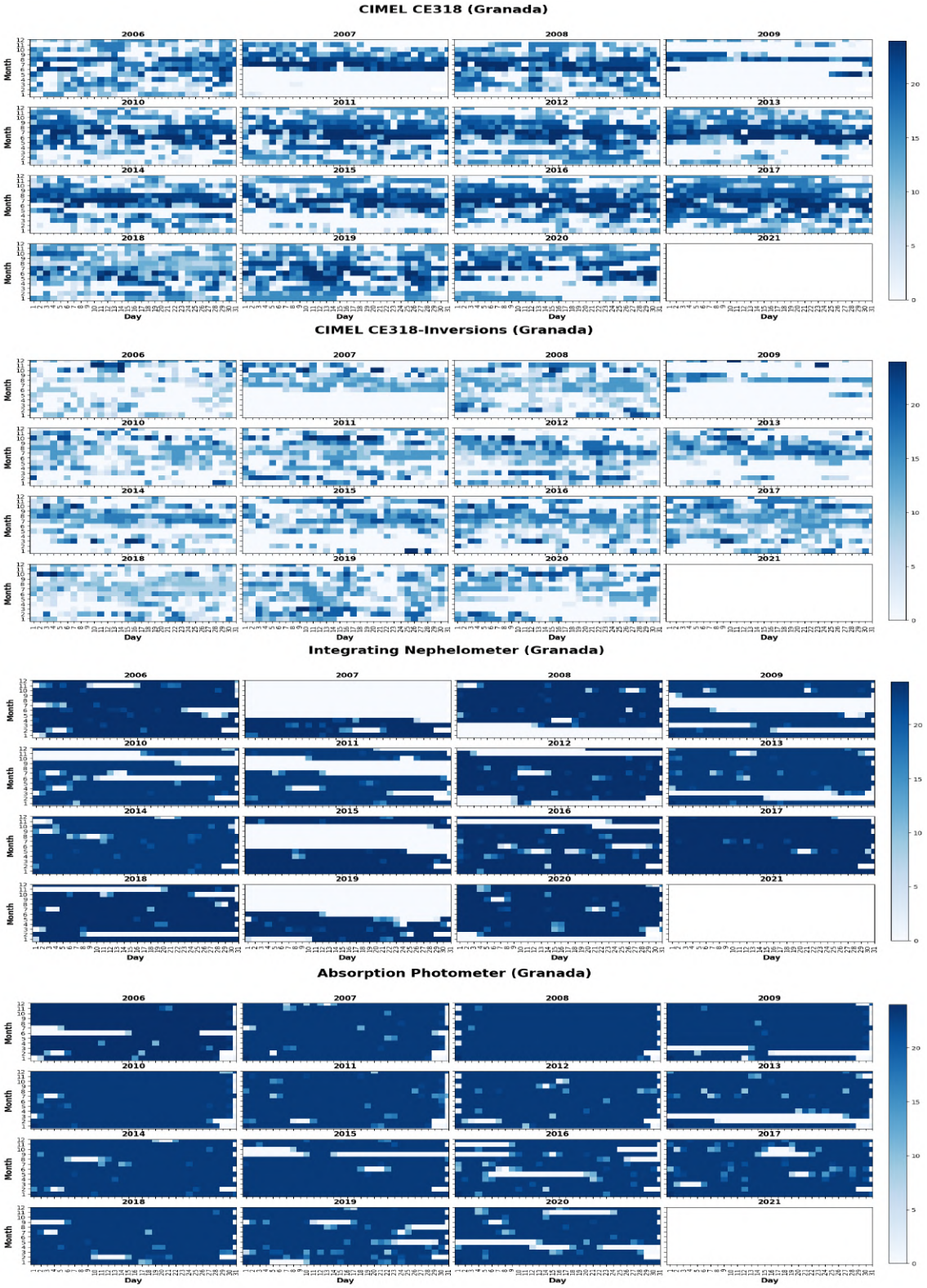

Fig. 17. Matrices of data available in Granada. Daily data is presented per month and day for the CIMEL CE318 and its inversions, Integrating Nephelometer, and Absorption Photometer.

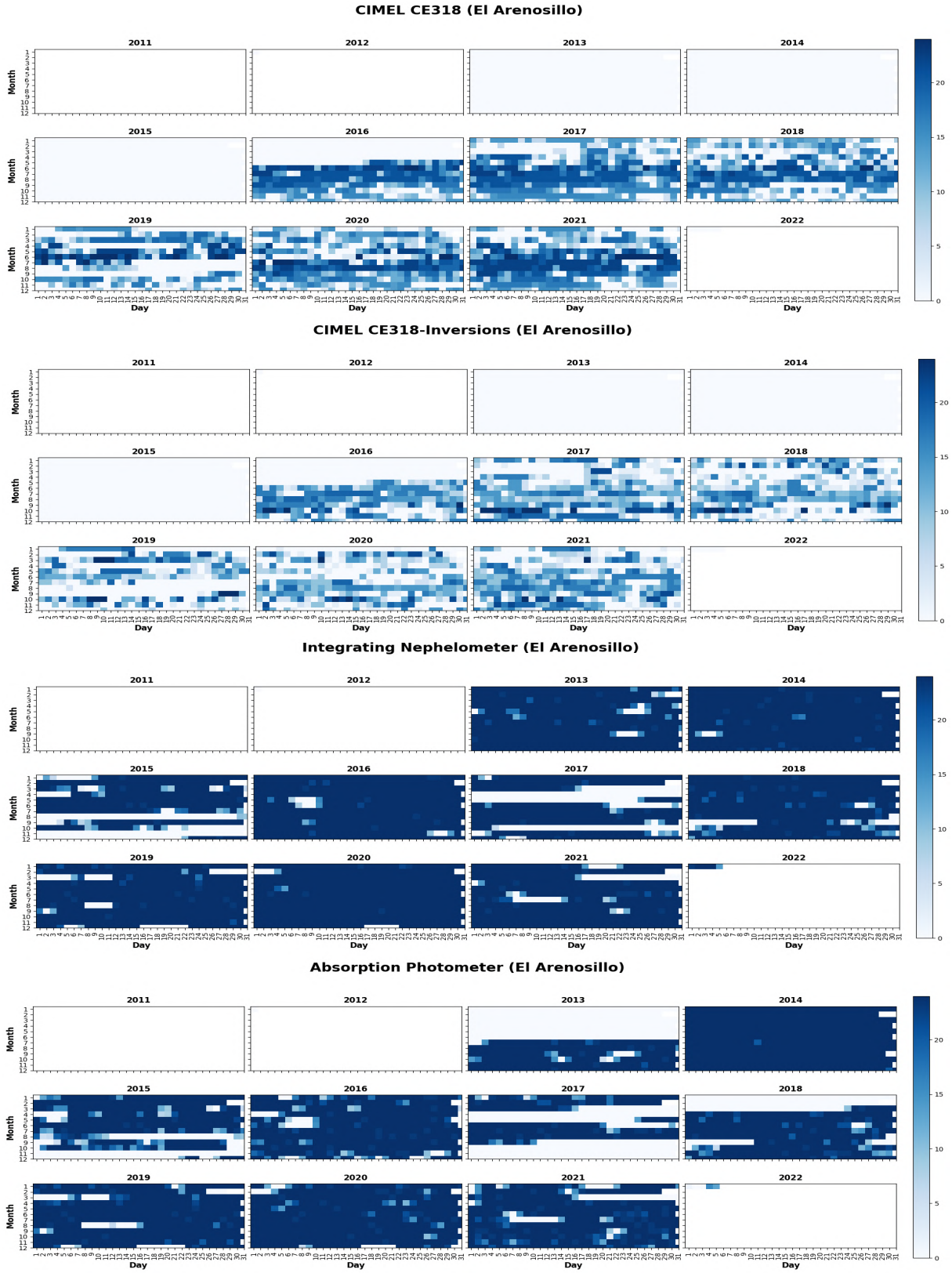

Fig. 18. Matrices of data available in El Arenosillo. Daily data is presented per month and day for the CIMEL CE318 and its inversions, Integrating Nephelometer, and Absorption Photometer.

	Granada							El Arenosillo						
Variable	Test	WIN	SPR	SUM	AUT	YEAR	SS	Test	WIN	SPR	SUM	AUT	YEAR	SS
AOD	MK1	D	D	NT	D	D	D	MK1	NT	NT	NT	D	NT	NT
	MK2	D	D	NT	D	D		MK2	NT	NT	I	D	D	
	MK3	D	D	NT	D	D		MK3	NT	NT	NT	D	NT	
σ_{sp}^{670}	MK1	D	D	D	D	D	D	MK1	I	I	NT	NT	I	I
	MK2	D	D	D	D	D		MK2	I	I	NT	I	I	
	MK3	D	D	D	D	D		MK3	I	I	NT	I	I	
σ_{ap}^{670}	MK1	D	D	D	D	D	D	MK1	NT	D	D	D	D	D
	MK2	D	D	D	D	D		MK2	NT	D	D	D	D	
	MK3	D	D	D	D	D		MK3	NT	D	D	D	D	
σ_{ep}^{670}	MK1	D	D	D	D	D	D	MK1	I	NT	NT	NT	I	NT
	MK2	D	D	D	D	D		MK2	I	NT	NT	NT	I	
	MK3	D	D	D	D	D		MK3	I	NT	NT	NT	NT	
SSA_{Situ}	MK1	I	NT	I	I	I	NT	MK1	I	I	I	I	I	I
	MK2	I	NT	I	I	I		MK2	I	I	I	I	I	
	MK3	NT	NT	I	I	NT		MK3	I	I	I	I	I	
SSA_{Col}	MK1	I	I	I	NT	I	NT	MK1	D	NT	I	I	NT	NT
	MK2	I	I	I	I	I		MK2	D	NT	I	I	NT	
	MK3	NT	NT	NT	NT	NT		MK3	D	NT	NT	I	NT	
SAE	MK1	NT	NT	NT	NT	I	NT	MK1	D	D	D	D	D	D
	MK2	D	NT	I	D	I		MK2	D	D	D	D	D	
	MK3	NT	NT	NT	NT	NT		MK3	NT	D	D	D	D	
AE	MK1	I	I	NT	NT	I	NT	MK1	D	NT	NT	NT	D	NT
	MK2	I	I	NT	NT	I		MK2	D	NT	NT	NT	D	
	MK3	I	I	NT	NT	I		MK3	D	NT	NT	NT	NT	

Table 4. Trends results using total data are displayed for both stations. The seasons are abbreviated, and their individual results are presented first for each implemented test (MK1 = Original Mann-Kendall, MK2 = TFPW, and MK3 = VCTFPW). On the right side of the dividing line, the annual trend is shown, and the statistical significance of the variable is represented in a box.

To understand the trend analysis, it is necessary to consider the difference between in-situ and column measurements, as differences between these provide information about changes in aerosol behavior across the atmospheric layers being studied. In this way, we analyze the results variable by variable for both stations[4][5].

For the Granada station, when possible, the obtained in-situ variable results will be compared with [14] or [15]. It should be noted that these studies span a duration of roughly 10 years with a different and smaller data population than the used in this work. While in El Arenosillo station, the lower amount of column data will be a significant bias factor in the found trends when comparing with other authors results, in [17] and [14] although the El Arenosillo station is not studied explicitly, results of general trends for the European continent are presented based on studies from a large number of stations.

[4]It should be noted that the uncertainty of the slope is presented within the regression equation, an uncertainty higher than the slope value itself is consequence of a non-trend result for the variables as it is reflected in Table 4.

[5]Only annual plots are shown, to see the seasonal trend analysis for each variable go to DRIVE link.

- **Scattering coefficient**:
  - Granada: a clear downward trend (-1.0 ± 0.1) yrs^{-1}Mm^{-1} is visually evident in Fig. 19, except for several years such as 2007 and 2015 (with limited available data) or 2017. This downward trend corresponds to the results of the Table 4 tests, which are consistent in all cases. In the later years of the study, a decrease in data dispersion is observed, reflected in the narrowing of the box plots. Comparing with [14], different results are obtained, as the authors of that work do not find an appreciable trend for the coefficient. This difference may be due to the use of different databases. On the other hand in [15] a decreasing trend is obtained for σ_{sp}^{670} in agreement with the results of this work.
  - El Arenosillo: in this case, there is a slight increasing trend, (0.4 ± 0.2) yrs^{-1}Mm^{-1}, throughout the studied time series (except for the years with limited data) Fig. 19. There is little statistical deviation from the studied population, which agrees with the results of the tests in Table 4 indicating an increase. In [17] a decreasing trend is obtained for European stations, the disagreement may come from the difference in data bases used and the general result obtained by the authors.
- **AOD**:
  - Granada: for AOD, a decreasing trend is also observed in Fig. 19 $(-1.9 \pm 0.4) \cdot 10^{-3}$ yrs^{-1}, showing agreement with what happens in the atmospheric surface layer as seen in the in-situ measurement of the extinction coefficient (Fig. 20). However, it does not follow such a clear trend with a much smaller normalized slope, indicating that in the upper layers, there would be a smaller decrease in the coefficient. In the Table 4 statistical tests, a decreasing trend is found, except for the summer season, where the values remain constant in the time series.
  - El Arenosillo: similar to the extinction coefficient trend in Fig. 20, we find a lack of trend for AOD despite referring to different atmospheric layers, with a larger dispersion Fig. 19. The statistical study in Table 4 indicates a lack of trend.

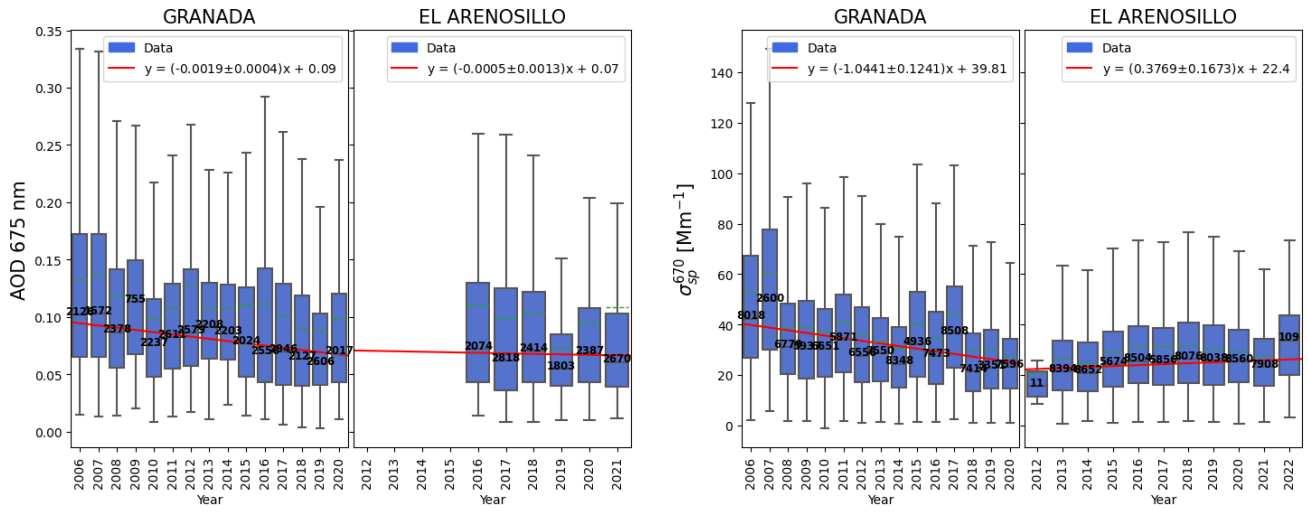

a) AOD 675 nm **b)** σ_{sp}^{670}

Fig. 19. AOD and σ_{sp}^{670} total trends in each station.

- **Absorption coefficient**:
  - Granada: a clearer downward trend (-0.45 ± 0.04) yrs^{-1}Mm^{-1}, is also observed in Fig. 20[6], with the exception of an increase in absorption for the year 2014 and the subsequent sub-trend around those years, but the downward factor remains. The results of the Table 4 tests are consistent with the observations, showing a consistent downward trend with a progressive decrease in data dispersion. In this case, the results are in agreement with those presented in [14].
  - El Arenosillo: a behavior opposite to the scattering coefficient is visible in Fig. 20. In this case, there is a clear decrease in the coefficient values (-0.09 ± 0.02) yrs^{-1}Mm^{-1}, and a higher data dispersion, as reflected in the results of the tests in Table 4. Comparing with the results in [17] a similar decreasing trend is found, therefore being in agreement with the results presented in this work.
- **Extinction coefficient**:
  - Granada: since the scattering and absorption coefficients are decreasing, it is logical to observe a similar trend in Fig. 20 (-1.5 ± 0.2) yrs^{-1}Mm^{-1}, as confirmed by the statistical tests in Table 4. The years with the most discrepancy from the general trend are the same as those observed for the scattering coefficient, as it has the greatest influence.
  - El Arenosillo: there is very little data dispersion along with a practically constant behavior Fig. 20, resulting from the different trends found for the scattering and absorption coefficients on which the extinction coefficient depends Eq. 4. This lack of trend is evidenced by the majority of NT results found in Table 4.

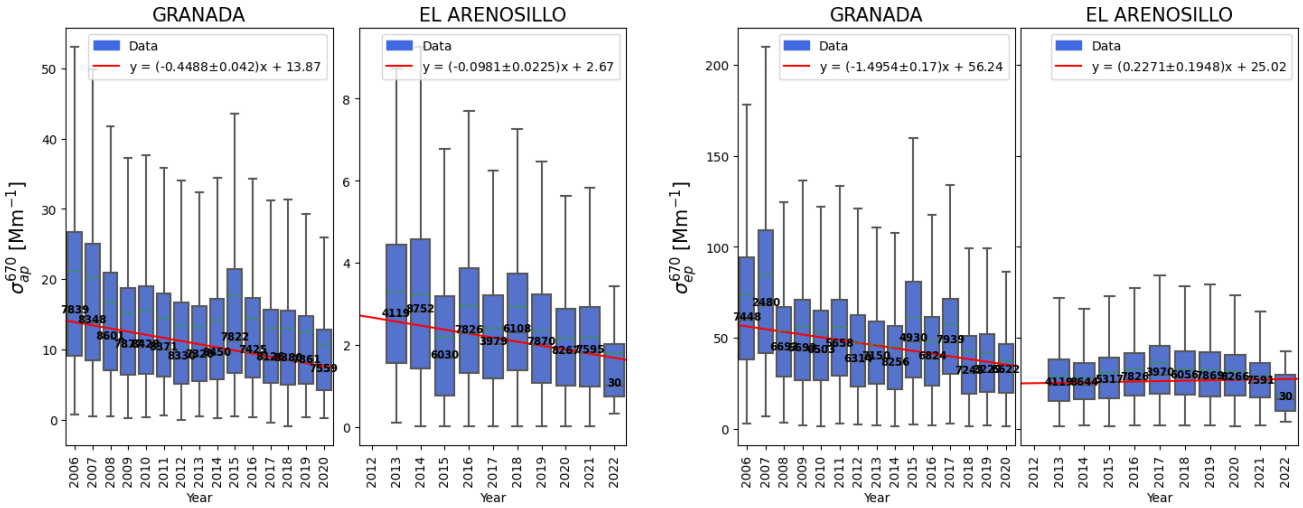

a) σ_{ap}^{670} **b)** σ_{ep}^{670}

Fig. 20. σ_{ap}^{670} and σ_{ep}^{670} total trends in each station.

- **SSA column**:
  - Granada: the trend observed in Fig. 21 is slightly increasing, with a significant decrease around 2014, resulting in a notable increase in data dispersion. The presence of this sub-trend causes the Table 4

[6] Absorption coefficient exhibits a significance difference in scale values from one station to another, hence a different y-axis is used in regards of a better visualization of data.

statistical tests to not find a clear overall trend. One possible reason for this decrease in SSA in the upper layers could be explained by sporadic climatic phenomena that contribute to an increase in the proportion of absorption in those layers, such as an increase in natural coarse mineral dusts.

- El Arenosillo: in Fig. 21, a globally constant behavior is observed, but with a slight sub-trend in 2019, resulting in a decrease in the scattering-to-absorption ratio (although scattering remains dominant). The data dispersion is small, and the trends found in Table 4 indicate a lack of clear trend.

▪ **SSA in-situ**:

- Granada: when comparing the column results with the surface measurements in Fig. 21, we see that the trend is slightly increasing in a similar manner. The main difference, besides having lower values, is the absence of the sub-trend observed in 2014. Instead, there is a slight decrease in comparison, which reinforces the hypothesis that the responsible phenomenon is located in layers that are not as superficial. Additionally, there is no increase in data dispersion during those years. In 2017, an atypical increase is observed due to the aforementioned errors in the nephelometer. The results of the Table 4 tests conclude that there is no clear overall trend. This is not in line with the findings of [14], as they report a slight increase. Judging by the results of the used tests, it seems to indicate that considering more years in the study would account for the discrepancy, as the valid trend results correspond to increases.
- El Arenosillo: for the surface layer, this is profoundly different. With a small data dispersion, there is a clear increasing trend observed in Fig. 21 $(5 \pm 0.7) \cdot 10^{-3}$ yrs^{-1}, and supported by the homogeneity of the statistical tests in Table 4. The explanation can be found in the results of the absorption and scattering coefficients: as the proportion of scattering increases and absorption decreases, it is logical that the SSA, as defined in Eq. 1, increases. In [17] or [14], authors identify a decreasing trend for European stations in regards of SSA, thus not corresponding to the increasing trend found, the reasons are the same aforementioned.

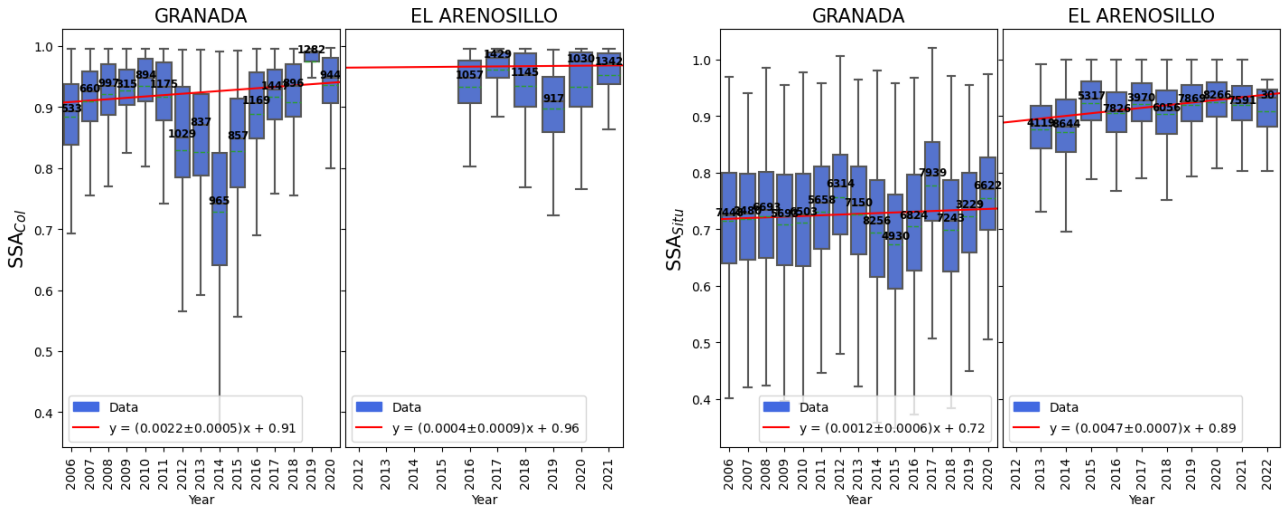

a) SSA Column **b)** SSA in-situ

Fig. 21. SSA total trends for both measurements methods in each station.

▪ **SAE**:

- Granada: for the Scattering Ångström Exponent, no clear trend is observed Fig. 22, the main reason for this is found in the year 2017 in which there is a considerable decrease indicating a higher amount of

aerosols of type coarse when the global trend is predominance of fine particles as explained previously, in addition the dispersion of the data suffers a slight increase as the years of study progress. This is reflected in the trends of Table 4 where the predominant result is NT which is in disagreement with the slight increasing trend found by [14].

- El Arenosillo: a clear decreasing trend has been found both in Fig. 22 and in the tests Table 4 $(2 \pm 0.7) \cdot 10^{-2}$ yrs^{-1}, despite the high data dispersion. This decreasing trend would indicate the progressive presence of increasingly larger aerosols, i.e., coarse particles, contributing to a higher proportion of scattering, which is consistent with the previous trends of the in-situ variables. In [17] a similar decreasing trend in SAE is found.

- **AE**:

  - Granada: for the Ångström Exponent, an increasing trend is observed in Fig. 22, but with a large dispersion of the data (without the existence of atypical values in the year 2017 compared to SAE), this large dispersion contributes to the statistical tests in Table 4 providing a lack of trend result (despite clear increasing trends in seasons such as winter or spring or the annual case).
  - El Arenosillo: although a slight decreasing trend could be interpreted based on the graph in Fig. 22, due to the limited amount of data in the study and their dispersion, when applying the tests, it is found that there is no generalized trend (except for winter data) Table 4.

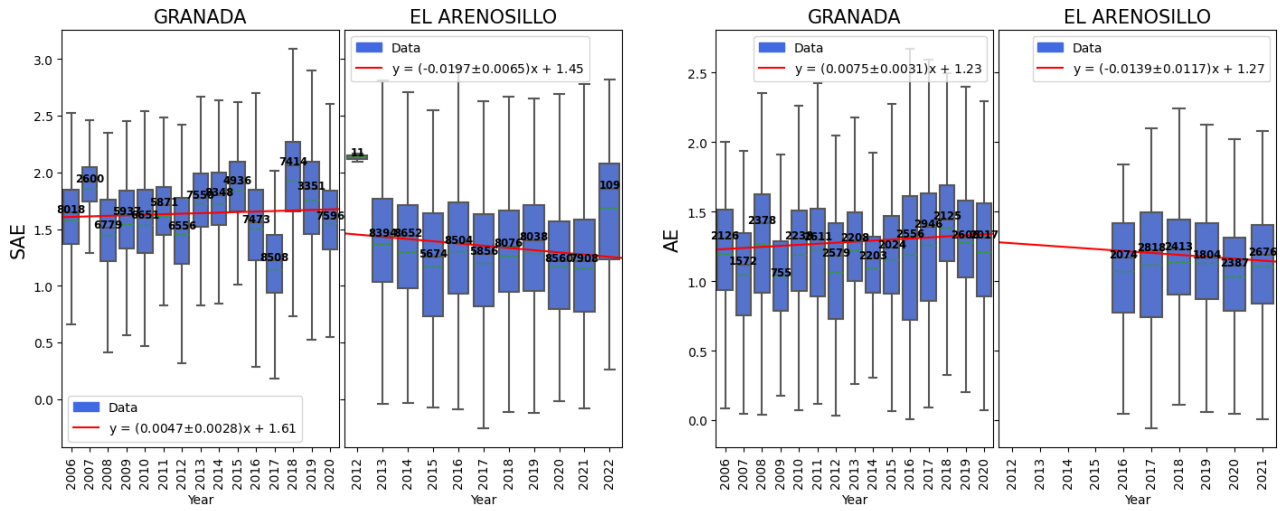

a) SAE **b)** AE

Fig. 22. SAE and AE total trends in each station.

In general, in Granada station (despite the existence of differences in small time periods), the existing trends of the column and in-situ methods are homogeneous for the variables studied in the comparison section.

Whereas at El Arenosillo station, a larger disparity between column and in-situ variables compared to the Granada station is exhibited. This highlights the significant influence of the measurement method on the observed trends. In addition to considering the local atmospheric conditions and the notable difference between the layers studied in terms of the aerosols' characteristics, the main reason for the notable inconsistency between in-situ and column trends could be the limited availability of column variable data, spanning only six years.

6.2.2. Simultaneous data

When the simultaneity of measurements is applied, a smaller amount of data is obtained. In Fig. 23 frequency matrices are represented in the same way as in the previous case. There are both fewer measurements and fewer years of study, the main reason being that we are equalizing the measurement frequency in the same time period of the remote sensing method with the in-situ method. Based on these simultaneous data, the same process of statistical trend analysis is conducted comparing both stations, figures of the data treatment are shown in Fig. 24. The results will be presented in Table 5 using the same format as the results obtained with the total data, differences found in the results are denoted with an asterisk (*).

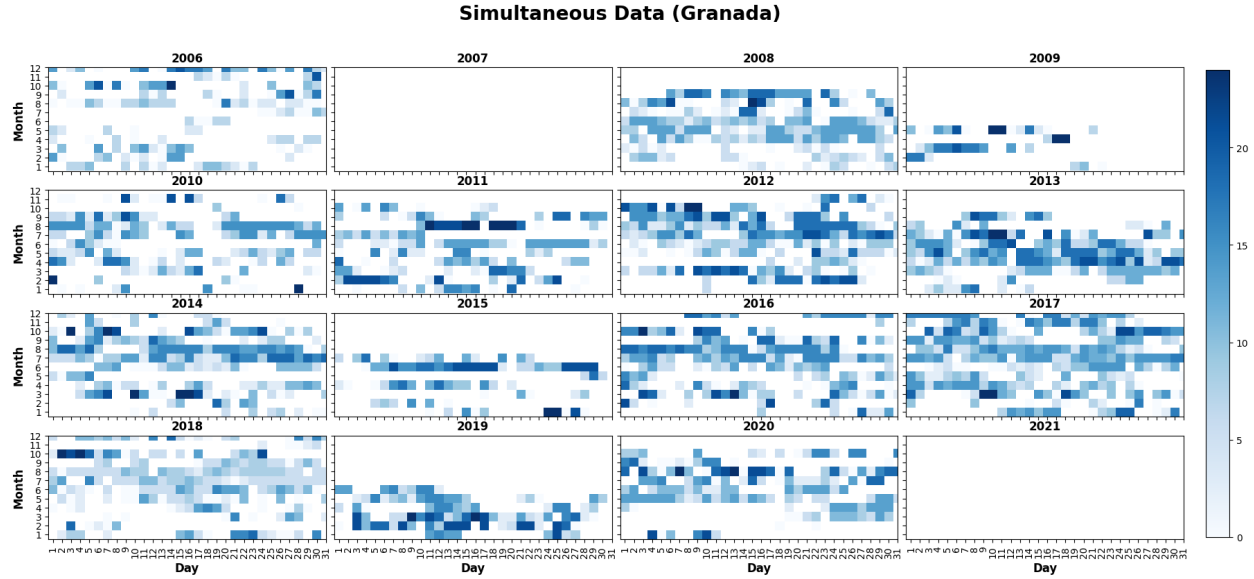

a) Granada.

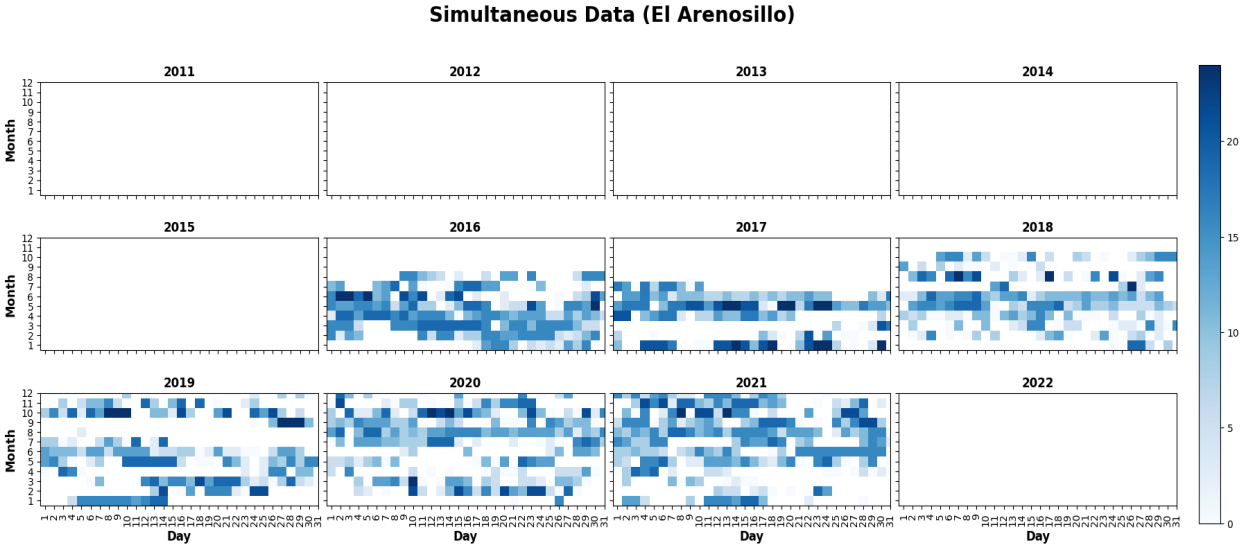

b) El Arenosillo.

Fig. 23. Matrices of available data after the simultaneity filter has been implemented for each station.

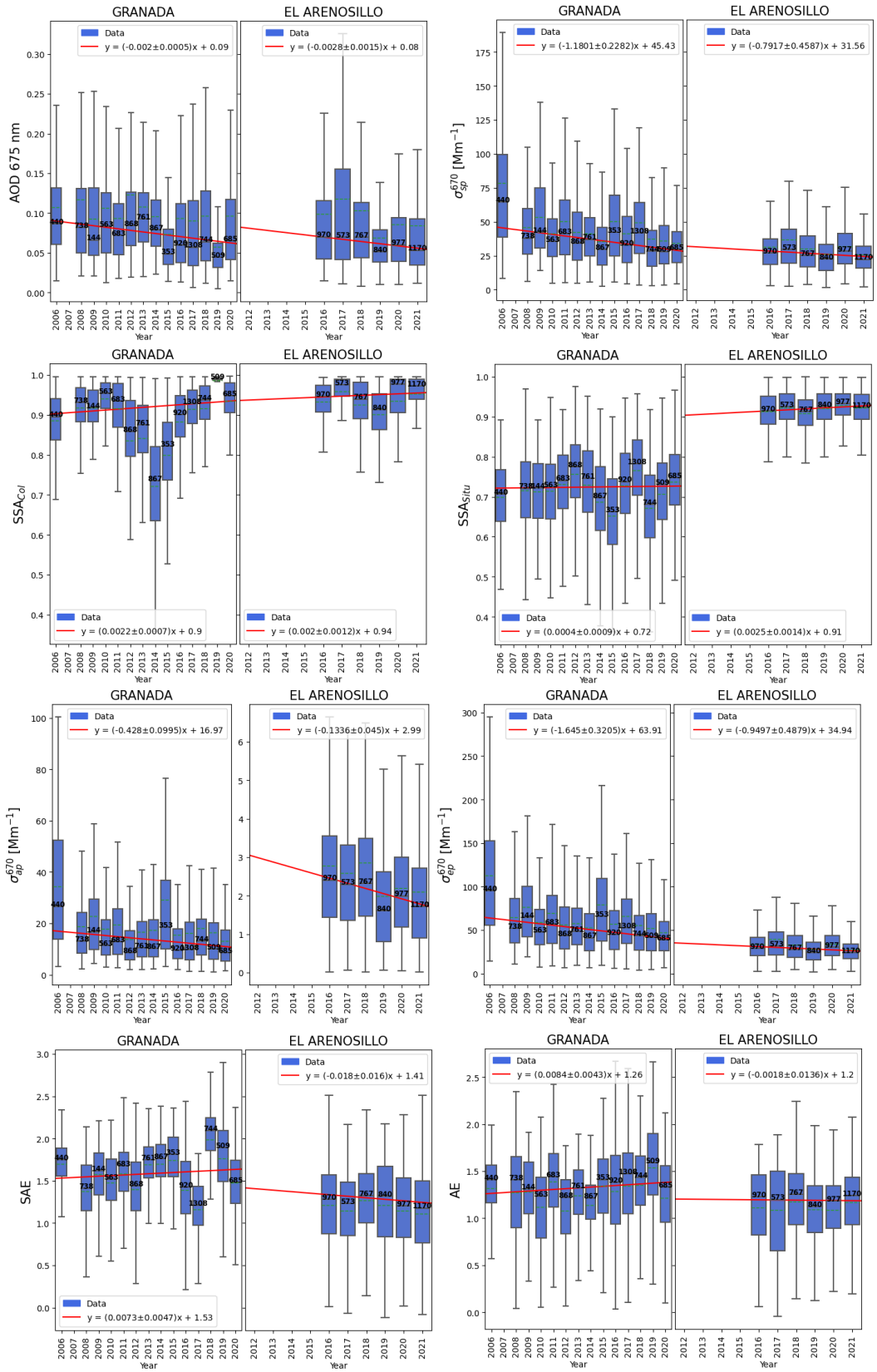

Fig. 24. Simultaneous trends for each aerosol variable found in Granada and El Arenosillo.

	Granada							El Arenosillo						
Variable	Test	WIN	SPR	SUM	AUT	YEAR	SS	Test	WIN	SPR	SUM	AUT	YEAR	SS
AOD	MK1	D	D	NT	D	D	D	MK1	NT	NT	NT	D	D*	NT
	MK2	D	D	NT	D	D		MK2	D*	I*	D*	D	D	
	MK3	D	D	NT	D	D		MK3	NT	NT	NT	D	D*	
σ_{sp}^{670}	MK1	D	D	D	D	D	D	MK1	NT*	D*	D*	D*	D*	D*
	MK2	D	D	D	D	D		MK2	NT*	D*	D*	D*	D*	
	MK3	D	D	D	D	D		MK3	NT*	D*	D*	D*	D*	
σ_{ap}^{670}	MK1	D	D	D	D	D	D	MK1	NT	NT*	D	D	D	NT*
	MK2	D	D	D	D	D		MK2	D*	D	D	D	D	
	MK3	D	D	D	D	D		MK3	NT	NT*	D	D	D	
σ_{ep}^{670}	MK1	D	D	D	D	D	D	MK1	NT*	D*	D*	D*	D*	D*
	MK2	D	D	D	D	D		MK2	NT*	D*	D*	D*	D*	
	MK3	D	D	D	D	D		MK3	NT*	D*	D*	D*	D*	
SSA_{Situ}	MK1	I	NT	I	NT	I*	NT	MK1	I	NT*	I	I	I	NT*
	MK2	I	NT	I	NT	I*		MK2	I	NT*	I	I	I	
	MK3	I*	NT	NT*	NT*	I*		MK3	NT*	NT*	I	I	I	
SSA_{Col}	MK1	I	I	I	I*	I	NT	MK1	D	I*	I	I	I	NT
	MK2	I	I	I	I	I		MK2	D	I*	I	I	I	
	MK3	I*	I*	NT	NT	NT*		MK3	D	NT	I*	I	I	
SAE	MK1	D*	I*	NT	NT	D*	NT	MK1	NT*	NT*	D	D	D	NT*
	MK2	D	I*	I	D	D*		MK2	I*	NT*	D	D	D	
	MK3	NT	NT	NT	NT	NT		MK3	NT*	NT*	NT*	D	D	
AE	MK1	I	I	NT	I*	I	I*	MK1	D	NT	NT	I*	NT*	NT
	MK2	I	I	D*	I	I*		MK2	D	D*	D*	I*	I*	
	MK3	I	I	NT	I*	I		MK3	D	NT	NT	I*	NT	

Table 5. Granada and El Arenosillo trends results using Simultaneous data. An asterisk (*) indicates a change in the trend provided by the tests compared to the results obtained with total data.

Based on the results of the tests shown in Table 5 and the trends observed in Fig. 24 (where the lack of measurement years and decrease in observations become evident), a further analysis is conducted by distinguishing each station according to the variables that exhibit differences in their trends when applying the filter:

- Granada station.
  - Only the difference in AE is found, as it changes from a no trend situation to a slightly increasing one, due to an increase in seasonal homogeneity (MK3 yields an increasing result in Autumn in Table 5).
  - The rest of variables remain their previously found trends, worth mentioning are the cases of AOD, σ_{sp}^{670}, σ_{ap}^{670} and σ_{ep}^{670} in which an absolute homogeneity is found for all statistical trends and seasons when compared to total trends. For SAE, and both SSAs, although their respective original (**ss**) are unchanged, they exhibit changes in the trends result, in particular SSA_{Situ} has a major change in the seasonal and annual trends, but remains with an overall no trend result.

In Granada most of the **(ss)** results remain unmodified, this can be explained by the fact that despite applying a simultaneity filter as observed in Fig. 23, the measurements at the Granada station are still evenly distributed over a considerable number of years. This ensures that the reliability of the identified trends is not significantly affected as seen in the figures where the Theil-Sen's estimator is applied (Fig. 24).

- El Arenosillo station.
  - Remote sensing variables (AOD, SSA_{Col} and AE) all keep their previous found trends **(ss)**, but a remarkable change in lesser potent statistical tests is observed throughout Table 5, in particular for SSA_{Situ} a slight increase in seasonal homogeneity is gained in Summer but insufficient for a valid trend, something similar is found in AOD in the annual case but the persistent lack of homogeneous seasonal results leads to a non-trend result.
  - For the scattering coefficient σ_{sp}^{670} a decreasing trend is found (with the exception of Winter), in this case the simultaneity filter hinders greatly the number of data used, thus explaining the change in trends in Table 5 from increasing to decreasing, in Fig. 24 the difference in the overall trend can be seen, which compared to the total one in Fig. 19, it suffers a radical trend downshift.
  - The absorption coefficient σ_{ap}^{670} also exhibits change in **(ss)**, the statistical tests yield a non-trend result derived from a loss in homogeneity in Winter and Spring.
  - In the extinction coefficient σ_{ep}^{670} a generalized change in tests results is observed in Table 5 as well as in the σ_{sp}^{670} case, leading to a decreasing trend in accordance of what can be deduced from σ_{sp}^{670} and σ_{ap}^{670} aforementioned trends.
  - SSA_{Situ} changes from a clear increasing trend when studied employing the total data to a non-trend one, this is remarkable as a large proportion of the implemented tests provide increasing tests in Table 5, the change in trend is once again due to a loss in homogeneity in the more powerful test (MK3) in consequence of the lack of sufficient data to ensure robust statistical tests.
  - SAE shifts to a non-trend result, just as SSA_{Situ}, the reason behind this change is a lack in seasonal homogeneity as seen in Table 5, where the original clear decreasing trend (Fig. 22) is replaced by a more constant slope, in Fig. 24 the annual trend is shown (it should be noted that this case keeps the decreasing trend but the overall (**ss**) is determined based on the seasonal trends not shown).

At El Arenosillo station, the opposite occurs compared to Granada. The results of the tests and the trends undergo widespread changes, mainly in the in-situ variables (see Table 6). This is due to the existence of an insufficient study period for the trends, which is further aggravated when applying simultaneity.

This provides us with important results regarding the treatment of data from databases (using simultaneous or total measurements) for conducting studies and comparing measurement methods for the obtained results:

1. When using simultaneous data, similar results to the total measurements are obtained, as long as there is a sufficiently large statistical population of years. This will depend on the station and the data availability based on the functioning of the necessary instrumentation.
2. If there is not a wide range of study, a decrease in the homogeneity of the results is observed across different tests and stations, which contributes to an increase in the lack of identified trends.
3. In both studied cases, it has been found that the dispersion of the analyzed data is not significantly altered when the simultaneity filter is applied.

	Granada		El Arenosillo	
Variable	Total	Simult.	Total	Simult.
σ_{sp}^{670}	**D**	**D**	**NT**	**D***
σ_{ap}^{670}	**D**	**D**	**I**	**NT***
σ_{ep}^{670}	**D**	**D**	**NT**	**D***
SSA	**NT**	**NT**	**I**	**NT***
SAE	**NT**	**I***	**D**	**NT***

Table 6. Granada and El Arenosillo (**ss**) trends differences found for in-situ variables when comparing the simultaneity bias outcome. Note how all of El Arenosillo's simultaneous results differ from total data trends.

7. Conclusions

In this study, the in-situ and remote sensing measurement techniques for atmospheric aerosol properties have been compared. This comparison was conducted at the Granada and El Arenosillo stations, which have distinct climatic conditions and are affected by different aerosol sources.

Firstly, online databases AERONET (remote sensing) and WDCA (in-situ) were used to obtain the data, which were processed using Python-based programs. This processing involved filtering out erroneous measurement data, calculating derived variables from direct instrument measurements (SSA, AEE, SAE, and $\sigma_{ep}(\lambda)$) for the in-situ techniques, creating a database with a common temporal periodicity for both measurement techniques, and enabling the application of a simultaneity filter between the two methods.

Using SSA values obtained from both methods, it has been found that higher values are observed for remote sensing techniques compared to in-situ measurements, with a larger difference at the Granada station than at El Arenosillo. This indicates a predominance of scattering processes in the upper layers, while different results are observed for each station in the surface layer. In Granada, there is an abrupt difference where absorption processes become dominant, whereas at El Arenosillo, scattering remains dominant with negligible absorption. This suggests the presence of a significant amount of aerosols of anthropogenic origin linked to pollution, such as BC (from road traffic), biomass burning, or domestic heating emissions, which are characteristic of an urban environment like Granada compared to the rural and remote environment of El Arenosillo, where this sharp gradient in the dominant process is not observed.

The comparison of AE values between both methods reinforces these findings. In Granada, fine aerosols (mainly BC) predominate at the surface, while in the upper layers, their proportion decreases, giving way to a predominance of coarse aerosols that are more scattering. At the El Arenosillo station, there is a predominance of coarse aerosols when measured using the different techniques, in the whole atmospheric vertical column. In conclusion, the differences between atmospheric layers in terms of dominant aerosol processes and sizes depend largely on the presence of anthropogenic aerosols, leading to an amplification of these differences.

To further investigate the comparison between both measurement techniques, trends in the studied atmospheric variables were examined using Mann-Kendall tests to discern the presence of trends and the Theil-Sen's estimator for slope estimation. When considering the total data set, similar trends are found for the variables in both surface and upper layers, but only at the Granada station. This would indicate that there are larger differences in aerosol behaviours between the surface layer and those existing throughout the column for El Arenosillo. This can be explained by the lack of sufficient measurements, which introduces a significant bias in the results. In Granada, no noticeable trends are observed for SSA and AE, while decreasing trends are obtained for AOD and all of the coefficients studied. Whereas at El Arenosillo, the in-situ techniques show an increasing SSA, a decreasing SAE, increasing scattering and decreasing absorption, while no trends are observed for remote sensing techniques and the extinction coefficient, Table 4.

The need for sufficiently long study periods to ensure reliable trend comparisons is evident when implementing the simultaneity bias in the data. In Granada, the trends remain largely unaffected except for AE, while in El Arenosillo, where there are fewer years of study and a greater data loss due to the filter application, the trends change, particularly for all in-situ variables, as the in-situ method is for more affected by simultaneity than remote sensing Table 5 & Table 6.

Improvements to this work could be carried out in the lines of expanding the time period of study at El Arenosillo station, seeking to contrast if the differences found when applying the simultaneous filter in the trends are still present or vanish, as a sufficient time period is found and used.

In future lines of research, it is proposed to expand this comparison between in-situ and remote sensing techniques to other stations, that have data availability in the databases used for both methods (such as the Madrid, Izana, Barcelona or Montsec stations in Spain). Since, as has been demonstrated, there is a strong temporal and spatial dependency in the comparison between the techniques, stemming from the nature of atmospheric aerosols, therefore requiring an expansion of this comparison to other geographical locations.

8. Appendix: Phyton (Jupyter) code implemented and data availability

A flowchart illustrating the programs' working scheme is presented in Fig. 25, the programs and the used data are available in DRIVE link. The developed programs process the data from both measurement techniques, in order to obtain a single file with all the variables studied in the same period and temporal measurement frequency (data every 1 hour). This process is carried out as follows:

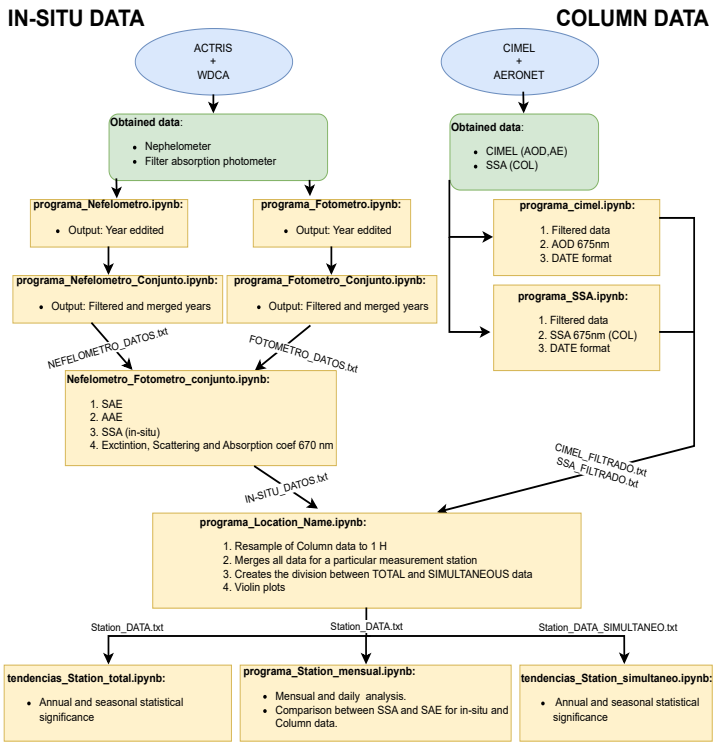

Fig. 25. Flowchart of the Pyhton (Jupyter) scripts developed.

- In-situ
  1. The data from the nephelometer and photometer (scattering and absorption coefficients) are separated and stored in separate files per year in the database. The first program is used in each case to filter the flags (NaN data from the database) and create date formats (mm, dd, yyyy, DATE, hh:mm:ss).
  2. All years for both instruments are merged into a single file, and the derived in-situ variables (SAE, AAE, SSA, and σ_{ep}^{670}) are calculated based on the available data.
- Remote sensing (column)
  1. For column method data, it is not necessary to calculate variables in the programs as the AOD data and used indirect measurements (SSA and AE) are already provided. However, they are stored in different files that need to be filtered for flags and processed prior to merging, using the same DATE format.
- The data from both methods are merged into a single file through an hourly resample at a measurement frequency of 1 hour (column data has a different hourly frequency). Once done, it is now possible to obtain data with simultaneous filtering and data without filtering. To achieve this, all measurements from different instruments that are not coincident are removed, which will have a greater effect on the in-situ data than on the column data.
- The following programs are used for trend analysis and comparison of variables according to the measurement techniques.

References

[1] Ogren J. A. *Comment on calibration and intercomparison of filter-based measurements of visible light absorption by aerosols.* Aerosol Sci Tech. 44, 589–591. 2010. DOI: https://doi.org/10.1080/02786826.2010.482111.

[2] Red Aeronet. NASA. URL: http://aeronet.gsfc.nasa.gov/.

[3] The World Data Centre for Aerosols (WDCA). Global Atmosphere Watch and NILU. URL: https://www.gaw-wdca.org.

[4] Borja-Aburto V. et al. *Mortality and ambient fine particulates in Southwest Mexico City; 1993–1995.* Environmental Health Perspectives 106, 849–855. 1999.

[5] Delfino R.J. et al. *Potential Role of Ultrafine Particles in Associations between Airborne Particle Mass and Cardiovascular Health.* Environ Health Persp vol. 113. No. 8 934-946. 2005.

[6] Forster P. et al. *IPCC. Climate Change 2021: The Physical Science Basis. Contribution of Working Group I to the Sixth Assessment Report of the Intergovernmental Panel on Climate Change.* IPCC. Cambridge University Press. 2021. DOI: 10.1017/9781009157896.009.

[7] Foyo-Moreno I. et al. *Estimating aerosol characteristics from solar irradiance measurements at an urban location in southeastern Spain.* Journal of geophysical research, Atmospheres, Volume 119, Issue 4, 27 February. 2014. DOI: https://doi.org/10.1029/2010JD014510.

[8] Héctor Rivera et al. *Variations in the physicochemical and optical properties of natural aerosols in Puerto Rico - Implications for climate.* Atmospheric Chemistry and Physics. 2018. DOI: https://doi.org/10.5194/acp-2018-791.

[9] Invernizzi G. et al. *Measurement of black carbon concentration as an indicator of air quality benefits of traffic restriction policies within the ecopass zone in Milan. Italy.* Atmos. Environ. 45, 3522-3527. 2011.

[10] Jing Li et al. *Scattering and absorbing aerosols in the climate system.* Nat Rev Earth Environ 3, 363–379. 2022. DOI: https://doi.org/10.1038/s43017-022-00296-7.

[11] Johannes Quass et al. *Robust evidence for reversal of the trend in aerosol effective climate forcing.* Atmos. Chem. Phys., 22, 12221–12239. 2022. DOI: https://doi.org/10.5194/acp-22-12221-2022.

[12] Lyamani H. et al. *Black carbon aerosols over an urban area in south-eastern Spain: Changes detected after the 2008 economic crisis.* Atmospheric Environment Volume 45, Issue 35, November 2011, Pages 6423-6432. 2011. DOI: https://doi.org/10.1016/j.atmosenv.2011.07.063.

[13] M. Collaud Coen et al. *Effects of the prewhitening method, the time granularity, and the time segmentation on the Mann–Kendall trend detection and the associated Sen's slope.* Atmospheric Chemistry and Physics. 2020. DOI: https://doi.org/10.5194/amt-13-6945-2020.

[14] M. Collaud Coen et al. *Multidecadal trend analysis of in situ aerosol radiative properties.* Atmospheric Chemistry and Physics. 2020. DOI: https://doi.org/10.5194/acp-20-8867-2020.

[15] Marco Pandolfi et al. *A European aerosol phenomenology – 6: scattering properties of atmospheric aerosol particles from 28 ACTRIS sites.* Atmos. Chem. Phys., 18, 7877–7911. 2018. DOI: https://doi.org/10.5194/acp-18-7877-2018.

[16] Mijin Kim et al. *Optimal Estimation-Based Algorithm to Retrieve Aerosol Optical Properties for GEMS Measurements over Asia.* Remote sens. 2018, 10(2), 162. 2018. DOI: https://doi.org/10.3390/rs10020162.

[17] Mortier A. et al. *Evaluation of climate model aerosol trends with ground-based observation over the last 2 decades- an AeroCom and CMIP6 analysis.* Atmos. Chem. Phys., 20, 13355–13378. 2020. DOI: https://doi.org/10.5194/acp-20-13355-2020.

[18] Pope CA et al. *Particulate air pollution as predictor of mortality in a prospective study of US adults.* American Journal of Respiratory and Critical Care Medicine, 1995, 151:669–674. 1995.

[19] Rotstayn L. D. et al. *Projected effects of declining aerosols in RCP4.5: unmasking global warming?* Atmos. Chem. Phys., 13, 10883– 10905. 2013. DOI: https://doi.org/10.5194/acp-13-10883-2013.

[20] S. Solomon et al. *IPCC. Contribution of Working Group I to the Fourth Assessment Report of the Intergovernmental Panel on Climate Change.* IPCC. Cambridge University Press. 2007.

[21] Sebastian Düsing et al. *Measurement report: Comparison of airborne in-situ measured, lidar-based, and modeled aerosol optical properties in the Central European background – identifying sources of deviations.* Atmos. Chem. Phys., 21, 16745–16773. 2021. DOI: https://doi.org/10.5194/acp-21-16745-2021.

[22] Stohl A. et al. *Evaluating the climate and air quality impacts of short-lived pollutants*. Atmos. Chem. Phys. 15, 10529–10566, 2015. DOI: https://doi.org/10.5194/acp-15-10529-2015.

[23] T. F. Stocker et al. *IPCC. Contribution of Working Group I to the Fifth Assessment Report of the Intergovernmental Panel on Climate Change, in Summary for Policymakers in Climate Change*. IPCC. Cambridge University Press. 2013.

[24] Toledano C. et al. *Aerosol optical depth and Ångström exponent climatology at El Arenosillo AERONET site (Huelva, Spain)*. Royal Meteorological Society, Vol. 133, issue 624. 2007. DOI: https://doi.org/10.1002/qj.54.

[25] Valenzuela A. et al. *Aerosol properties retrieved from sky radiance at the Principal Plane for nonspherical particles*. IV Reunión Española de Ciencia y Tecnología del aerosol – RECTA 2010. 2010.

[26] Valenzuela A. et al. *Aerosol scattering and absorption Angström exponents as indicators of dust and 2 dust-free days over Granada (Spain)*. Atmospheric Research Volume: 154 Pages: 1-13 Published: 2015. 2015. DOI: 10.1016/j.atmosres.2014.10.015.

[27] Vratolis S. et al. *Comparison and complementary use of in situ and remote sensing aerosol measurements in the Athens Metropolitan Area*. Atmospheric Environment Volume 228, 1 May 2020, 117439. 2020. DOI: https://doi.org/10.1016/j.atmosenv.2020.117439.

[28] Yuchen Shi et al. *Atmospheric aerosol particle size distribution from Lidar data based on the lognormal distribution mode*. Heliyon Volume 8, Issue 8, August 2022, e09975. 2022. DOI: https://doi.org/10.1016/j.heliyon.2022.e09975.

[29] E Andrews. *Continuous Light Absorption Photometer (CLAP) Instrument Handbook*. US Department of Energy. 2022. DOI: DOE/SC-ARM-TR-280.

[30] ACTRIS data base. European Union. URL: https://www.actris.es.

[31] CIMEL CE318-T. Retrieved 13:37, June 26, 2023. URL: https://www.cimel.fr/solutions/ce318-t/.

[32] Petr Chelk and James A. Coakley Jr. *Aerosols and Climate*. Science. Vol 183, Issue 4120 pp. 75-77. 1974. DOI: https://doi.org/10.1126/science.183.4120.75.

[33] Zieger Paul Christoph. *Effects of relative humidity on aerosol light scattering*. ETH Zürich. 2011. DOI: https://doi.org/10.3929/ethz-a-006668068.

[34] EPA commission. *Air Quality Criteria for Particle Matter*. Environmental Protection Agency (EPA) US. 2004.

[35] Javier Villar Contreras. *Estudio de cierre entre las propiedades microfísicas, químicas y ópticas del aerosol atmosférico en Sierra Nevada y Granada*. University of Granada. 2019.

[36] Wikipedia contributors. *Box plot*. Wikipedia, The Free Encyclopedia. Retrieved 17:19, June 22, 2023. URL: https://en.wikipedia.org/w/index.php?title=Box_plot&oldid=1158421606.

[37] SXin Dang et al. *Theil-Sen Estimators in a Multiple Linear Regression Model*. University of Mississippi and Yale University.

[38] DEIMS-SDR. *Sierra Nevada / Granada (ES- SNE) - Spain*. URL: https://deims.org/e51cee43-dc12-4545-8e5b-dad35431e3f7.

[39] Esther Coz Diego. *Caracterización Química y Morfológica del Aerosol Ambiental en las Fracciones PM10 y PM2.5 mediante Microscopía Electrónica de Barrido en Episodios de Contaminación Atmosférica de Origen Diverso*. University Carlos III de Madrid, Department of Science and Engineering of Madrid. 2008.

[40] Delene DJ and Ogren JA. *Variability of Aerosol Optical Properties at Four North American Surface Monitoring Sites*. Surface Monitoring Sites. J. Atmos. Sci., 59, 1135–1149. 2002.

[41] Xu X. Dockery DW Pope CA. *An association between air pollution and mortality in six US cities*. New England Journal of Medicine, 1993,329:1753–1759. 1993.

[42] José Vicente Díaz. *La red Aeronet*. URL: https://josevicentediaz.com/teledeteccion/la-red-aeronet/.

[43] J.A. Casquero-Vera et al. F. Rejano G. Titos. *Activation properties of aerosol particles as cloud condensation nuclei at urban and high-altitude remote sites in southern Europe*. Science of the Total Environment. 2020. DOI: https://doi.org/10.1016/j.scitotenv.2020.143100.

[44] Titos G et al. *Spatial and temporal variability of carbonaceous aerosols: Assessing the impact of biomass burning in the urban environment*. Sci TotalEnviron. 2017. DOI: 10.1016/j.scitotenv.2016.11.007.

[45] GAWSIS. Station Information System, Retrieved 14:34, July 5, 2023. URL: https://gawsis.meteoswiss.ch/GAWSIS/#/.

[46] Ideal Granada. URL: https://www.ideal.es/granada/201410/08/granada-entre-areas-afectadas-20141008125000.html?ref=https\%3A\%2F\%2Fwww.google.com\%2F.

[47] J L. et al. Guerrero-rascado. *Aerosol closure study by lidar, Sun photometry, and airborne optical counters during DAMOCLES field campaign at El Arenosillo sounding station, Spain.* Journal of geophysical research, Atmospheres, 26 January. 2011. DOI: https://doi.org/10.1029/2010JD014510.

[48] Theil H. *A rank-invariant method of linear and polynominal regression analysis (parts 1-3).* In Ned. Akad. Wetensch. Proc. Ser. A (Vol. 53, pp. 1397-1412). 1950.

[49] R.K. Chakrabarty H. Moosmüller and W.P. Arnott. *Aerosol light absorption and its measurement: A review.* Journal of Quantitative Spectroscopy and Radiative Transfer Volume 110, Issue 11, July 2009, Pages 844-878. 2009. DOI: https://doi.org/10.1016/j.jqsrt.2009.02.035.

[50] Md. Manjurul Hussain and Ishtiak Mahmud. *pyMannKendall: a python package for non parametric Mann Kendall family of trend tests.* The Journal of Open Software (JOSS). 2019. DOI: https://doi.org/10.21105/joss.01556.

[51] IISTA-CEAMA. University of Granada. URL: https://www.iista.es.

[52] HAZE instruments. *CLAP-10 image.* Retrieved 17:23, 5 July, 2023. URL: https://haze.si/.

[53] IPCC. *The Intergovernmental Panel on Climate Change.* United Nations. 2023. URL: https://www.ipcc.ch.

[54] Heintzenberg J, Raes F, and Schwartz S. *Atmospheric Chemistry in a Changing World: An Integration and Synthesis of a Decade of Tropospheric Chemistry Research.* The International Global Atmospheric Chemisty Project of the International Geosphere-Biosphere Programme, Chapter 4: Tropospheric Aerosols, Springer Verlag. 2003.

[55] Seinfeld JH and Pandis SN. *Atmospheric Chemistry and Physics: From Air Pollution to Climate Change.* Wiley, New York, 1326pp. 1998.

[56] Christopher Robert Kitchin. *Stars, Nebulae and the Interstellar Medium: Observational Physics and Astrophysics.* CRC Press. 1987.

[57] Theodore L.Anderson and John A.Ogren. *Determining Aerosol Radiative Properties Using the TSI 3563 Integrating Nephelometer.* Joint Institute for the Study of the Atmosphere and Oceans, University of Washington. 2007. DOI: https://doi.org/10.1080/02786829808965551.

[58] Kendall M. *Rank correlation measures.* Charles Griffin London. 202 15. 1975.

[59] MIMOSA-5. *Monitoring and Modelling of Stratospheric Aerosols with a Focus on the Impact of Volcanic Eruptions.* Intitut Royal D'Aeronomie Spatialede and European Commission. 2016. URL: https://cordis.europa.eu/article/id/175000-volcanoes-aerosols-and-climate.

[60] *Multi Angle Absorption Photometer (MAAP) and Particulate Soot Absorption Photometer (PSAP).* Centre for Atmospheric Science, Manchester University. URL: http://www.cas.manchester.ac.uk/restools/instruments/aerosol/maap/.

[61] Naranjo-Fernández, N. Guardiola-Albert, and H. et al. *Relevance of spatio-temporal rainfall variability regarding groundwater management challenges under global change: case study in Doñana (SW Spain).* Stoch Environ Res Risk Assess 34, 1289–1311. 2010. DOI: https://doi.org/10.1007/s00477-020-01771-7.

[62] OnlineMathLearning.com. *Box Plot.* 2022. URL: https://www.onlinemathlearning.com/box-plot.html.

[63] Zieger P. *Effects of relative humidity on aerosol light scattering. PhD Thesis. Diss. ETH No. 19659, 2011.* 2011.

[64] Stark M. et al. Panteliadis P. *Implementation of a low emission zone and evaluation of effects on air quality by long-term monitoring.* Atmos. Environ. 86, 113-119. 2014.

[65] Andreas Petzold. *Multi-Angle Absorption Photometry - A New Method for the Measurement of Aerosol Light Absorption and Atmospheric Black Carbon.* Forschungszentrum Jülich. 2004. DOI: http://dx.doi.org/10.1016/j.jaerosci.2003.09.005.

[66] McMurry P.H., X.Q. Zhang, and C.T.Lee. *Issues in aerosol measurement for optics assessments.* Journal of Geophys. Res. Atmos., 101, 19189-19197. 1996.

[67] Sen P.K. *Estimates of the regression coefficient based on Kendall's tau.* Journal of the American statistical association, 63(324), 1379-1389. 1968. DOI: https://doi.org/10.1080/01621459.1968.10480934.

[68] DONAIRE project. *Atmospheric Deposition in Natural and Anthropized Environments Over Northeastern Spain; Integrated Geochemical and Magnetic Characterization.* CSIC and IGME. URL: https://www.igme.es/DonaireProject/English/default.htm.

[69] Joseph M. Prospero. *Long-term measurements of the transport of African mineral dust to the southeastern United States: Implications for regional air quality.* Journal of geophysical research. Volume 104 Issue D13 pages 15917-15927. 1999. DOI: https://doi.org/10.1029/1999JD900072.

[70] Ana del Águila Pérez. *Spatial and temporal variability of aerosol properties at different altitudes in Sierra Nevada using in-situ techniques.* University of Granada. 2016.

[71] Ana del Águila Pérez. *Study of the air quality of Granada urban environment using in-situ techniques.* University of Granada. 2015.

[72] ThermoFisher Scientist. Retrieved 13:49, June 26, 2023. URL: https://www.thermofisher.com/order/catalog/product/MODEL5012.

[73] American Thoracic Society. *Adverse effects of crystalline silica exposure.* American Journal of Respiratory and Critical Care Medicine. 155, 761–768. 1997.

[74] M. N. Sai Suman et al. *Role of Coarse and Fine Mode Aerosols in MODIS AOD Retrieval: a case study over southern India.* National Atmospheric Research Laboratory. 2014. DOI: 0.5194/amt-7-907-2014.

[75] TSI. Retrieved 13:45, June 26, 2023. URL: https://tsi.com/discontinued-products/integrating-nephelometer-3563/.

[76] TSI. *Model 3563 Integrating Nephelometer.* TSI Incorporated Particle Instruments, USA. 1995. URL: https://gml.noaa.gov/aftp/aerosol/doc/inst/neph/tsi3563.pdf.

[77] Gloria Titos Vela. *Characterization of atmospheric aerosol particles using in-situ techniques: optical, chemical and hygroscopic properties.* University of Granada, GFAT and CEAMA. 2014.

[78] Adam Voiland. *Aerosols: tiny particles, big impact.* URL: https://earthobservatory.nasa.gov/features/Aerosols. NASA Earth Observatory. 2010.

[79] Chien Wang. *Impact of anthropogenic absorbing aerosols on clouds and precipitation: A review of recent progresses.* Atmospheric Research Volume 122, March 2013, Pages 237-249. 2013. DOI: https://doi.org/10.1016/j.atmosres.2012.11.005.

[80] James W.Flitzgerald. *Marine aerosols: A review.* Atmospheric Physics Branch. Naval Research Laboratory. Washington D.C. 20375-5000 U.S.A. 1990. DOI: https://doi.org/10.1016/0960-1686(91)90050-H.

[81] Kenneth T. Whitby. *The Physical Characteristics of Sulfur Aerosols. Atmospheric Environment.* Particle Technology Laboratory. Mechanical Engineering Department. University of Minnesota Minneapolis. MN 55455 U.S.A. 1977.

[82] S. YUE and C.Y WANG. *The Mann-Kendall Test Modified by Effective Sample Size to Detect Trend in Serially Correlated Hydrological Series.* Water Resources Management, v.18, p.201-218. 2004. DOI: http://dx.doi.org/10.1023/B:WARM.0000043140.61082.60.

[83] S. Yue et al. *The influence of autocorrelation on the ability to detect trend in hydrological series.* Hydrol. Proc., 16, 1807–1829. 2002. DOI: https://doi.org/10.1002/hyp.1095.

UNIVERSIDAD DE GRANADA

Facultad de Ciencias
Sección de Físicas

Propuesta de Trabajo Fin de Grado en Física

Tutor/a:	Gloria Titos Vela
Departamento y Área de Conocimiento:	Física de la atmósfera
Correo electrónico:	***gtitos@ugr.es***
Cotutor/a:	Alberto Cazorla Cabrera
Departamento y Área de Conocimiento:	Física de la atmósfera
Correo electrónico:	***cazorla@ugr.es***

Título del Trabajo: Efecto radiativo del aerosol atmosférico: comparación entre técnicas de medida

Tipología del Trabajo: *(Segun punto 3 de las Directrices del TFG aprobadas por Comisión Docente el 10/12/14)*

(Marcar con X)

1. Revisión bibliográfica		*4. Elaboración de nuevas prácticas de laboratorio*	
2. Estudio de casos teórico-prácticos	*x*	*5. Elaboración de un proyecto*	
3. Trabajos experimentales		*6. Trabajo relacionado con prácticas externas*	

Breve descripción del trabajo:

Las partículas de aerosol atmosférico son partículas sólidas o líquidas en suspensión en la atmósfera. Estas partículas son de gran importancia para el balance radiativo del planeta y por tanto para el clima y el cambio climático. Las partículas de aerosol afectan directamente al balance de energía del sistema Tierra-Atmósfera dispersando y absorbiendo la radiación solar. Los procesos de absorción y la dispersión de radiación por el aerosol dependen fuertemente de las fuentes de emisión y de los procesos atmosféricos a los que se ven sometidas las partículas, que determinan el tamaño de las mismas y su composición química. Existen diferentes técnicas de medida de las propiedades del aerosol que nos proporcionan información complementaria del impacto del aerosol en el clima. Por un lado, las técnicas de medida in-situ en superficie nos proporcionan un amplio abanico de medidas (composición química, tamaño, propiedades ópticas, etc) con alta resolución temporal (medidas minutales, 24/7), aunque limitadas a la capa atmosférica próxima a superficie. Por otro lado, las técnicas de teledetección pasiva nos proporcionan información de la columna atmosférica pero su resolución temporal está limitada (varias medidas al día y sólo con cielo despejado) y las variables medidas se limitan a propiedades ópticas del aerosol. Existen diversas redes internacionales de medida que se encargan de garantizar la calidad de los datos y su alta cobertura espacio-temporal. Para medidas in-situ, algunas de estas redes son ACTRIS (*Aerosols, Clouds and Trace gases Research Infraestructure*, Pandolfi et al., 2019), NFAN (*NOAA Federated Aerosol Network*, Andrews et al., 2019) o GAW (*Global Atmospheric Watch*, Laj et al., 2020), mientras que para teledetección pasiva podemos destacar la red AERONET (*Aerosol Robotic Network*, Holben et al., 1998). Estos datos se recogen en su mayoría en bases de datos abiertas como ebas (http://ebas.nilu.no) y AERONET (https://aeronet.gsfc.nasa.gov/).

Objetivos planteados:

En este Trabajo Fin de Grado se plantean los siguientes objetivos:

- Familiarización con redes internacionales de medida y bases de datos *open-access*
- Analizar la variabilidad temporal de las propiedades ópticas del aerosol atmosférico en función de la técnica de medida utilizada.
- Determinar el impacto en el balance radiativo según la técnica de medida utilizada.

Metodología:

Para alcanzar los objetivos propuestos, el/la estudiante

- Identificará de estaciones de medida con medidas simultáneas in-situ y teledetección pasiva durante al menos 5 años.
- Obtendrá datos de coeficientes de dispersión y absorción para las estaciones identificadas.
- Obtendrá datos de espesor óptico de aerosoles de la red AERONET para las estaciones identificadas.
- Descargará los datos de las bases de datos internacionales para las estaciones de medida identificadas con medidas simultáneas de ambas técnicas de medida.
- Aplicará unos tests de calidad para garantizar que la base de datos es robusta.
- Estudiará la variabilidad temporal de las propiedades ópticas del aerosol atendiendo a variaciones diurnas, mensuales, y anuales de acuerdo a la técnica de medida utilizada.
- Determinará, en los casos en que sea posible, si existe tendencia temporal a lo largo del periodo de estudio, prestando especial atención a la técnica de medida utilizada.

Bibliografía:

Andrews, E., et al., 2019. Overview of the NOAA/ESRL federated aerosol network. Bull. Am. Meteorol. Soc. 100, 123–135. https://doi.org/10.1175/BAMS-D-17-0175.1.

Holben et al., 1998. AERONET—A Federated Instrument Network and Data Archive for Aerosol Characterization. Rem. Sen. Env. 66-1, 1-16. https://doi.org/10.1016/S0034-4257(98)00031-5

Laj, P., et al., 2020. A global analysis of climate-relevant aerosol properties retrieved from the network of GAW near-surface observatories. Atmos. Meas. Tech., 2020, 1–70. https://doi.org/10.5194/amt-2019-499

Pandolfi, M., et al., 2018. A European aerosol phenomenology - 6: scattering properties of atmospheric aerosol particles from 28 ACTRIS sites. Atmos. Chem. Phys. 18, 7877–7911. https://doi.org/10.5194/acp-18-7877-2018.

A rellenar sólo en el caso que el alumno sea quien realice la propuesta de TFG
Alumno/a propuesto/a:

Granada, 12 de Mayo 2022

Sello del Departamento

Campus Fuentenueva
Avda. Fuentenueva s/n
18071 Granada
Tfno. +34-958242736
almartin@ugr.es

Comisión Docente de Físicas
Facultad de Ciencias